RESEARCH

Energy-momentum-consistent simulation of planar geometrically exact beams in a port-Hamiltonian framework

Philipp L. Kinon[1,2] · **Peter Betsch**[1] · **Simon R. Eugster**[2]

Abstract

We propose a new, port-Hamiltonian formulation for the highly nonlinear dynamics of planar geometrically exact beams, which are amenable to arbitrary large deformations and rotations. A structure-preserving spatial and temporal discretization procedure - using mixed finite elements and second-order time-stepping methods - is proposed. It is observed that the present approach is objective, locking-free and provides an exact discrete representation of the energy and angular momentum balance. By comparing the approach to a classical displacement-based scheme from the literature it is shown that the port-Hamiltonian formulation paves new ways for the design of energy-momentum schemes in computational mechanics. Numerical examples underline the applicability to flexible multibody systems and beneficial numerical performance.

Keywords Planar Simo-Reissner beam · Port-Hamiltonian systems · Flexible multibody systems · Structure-preserving discretization · Mixed finite elements · Locking

1 Introduction

Highly flexible slender structures, such as beams, strings, rods, or shells, are ubiquitous in complex natural and technical systems. Typically, they function as sub-modules within larger flexible multibody systems, which may also include rigid components or joints [1, 2]. The dynamic behavior of such systems can be highly complex due to nonlinear geometry and intricate material properties. Accurately simulating these systems is crucial, particularly for long-term behavior, where numerical dissipation or energetic inconsistencies can lead to unphysical results.

A central approach to describing large deformations in thin, highly flexible structures is the use of geometrically exact beam (GEB) models, also known as Simo-Reissner beams [3, 4] or special Cosserat rods [5]. These highly popular models [6–12] accurately capture large displacements and rotations without relying on linear approximations and remain a

---

✉ P.L. Kinon
philipp.kinon@kit.edu

1   Institute of Mechanics, Karlsruhe Institute of Technology (KIT), Otto-Ammann-Platz 9, 76131 Karlsruhe, Germany

2   Department of Mechanical Engineering, Eindhoven University of Technology (TU/e), 5600 MB Eindhoven, The Netherlands

highly active research topic [13–16]. For a comprehensive overview on beam modeling, see [17].

The port-Hamiltonian (PH) framework has proven to be a powerful method for modeling and controlling dynamical systems [18, 19]. By ensuring energetic consistency and enabling modular interconnections, the PH framework allows interactions between different physical domains — such as mechanics, electronics, and thermodynamics — to be unified within a single formalism. This approach has been successfully applied to infinite-dimensional dynamical systems [20–22] and various structural elements such as strings [23–25], plates [26, 27], and beams [28–31]. In the context of finite strain elasticity, velocity-stress formulations have been developed in [32, 33]. In [34] the application to a floating frame formulation is discussed. Starting from a discrete Lagrangian description, the PH approach is exploited in [35] for energy-shaping control.

Furthermore, structure-preserving discretization methods are crucial for the successful application of the PH framework in flexible multibody simulations. These methods ensure that the underlying energy balance equation is maintained at the discrete level, preventing numerical dissipation and energy inconsistencies. In particular, the spatial discretization of PH systems is commonly handled using the mixed finite element methods [24, 34, 36–38]. Similarly, time discretization plays a crucial role in capturing the evolution of system dynamics while preserving energetic consistency. Energy-preserving time discretization schemes, such as midpoint type methods, discrete-gradient approaches or projection-based schemes ensure that energy flows within the system are correctly simulated, which is particularly vital for long-term stability and control applications.

Schemes capable of preserving both energy and momentum are commonly termed EM schemes. Being a popular tool for the simulation of mechanical systems, notable works dealing with geometrically exact beams are for example [12, 39, 40].

1.1 Research gap

Despite the extensive research on both GEB models and the PH framework, there has been no prior work integrating these two approaches. This is surprising given that the PH framework is particularly well-suited for flexible multibody systems, where GEB formulations are often used. The combination of these two methodologies could provide a powerful tool for accurate and energy-consistent simulations of such systems.

Another critical challenge in the numerical simulation of slender mechanical structures is the phenomenon of transverse shear locking. This numerical stiffening effect arises during discretization, leading to unrealistically small deformations. While popular solutions such as selectively reduced integration [39] and mixed finite elements exist, shear locking has received little attention in the PH context. The only reference we are aware of is [41], which discusses mixed finite elements for Mindlin plates but does not address GEBs.

Additionally, existing geometrically nonlinear PH beam formulations [29, 30] rely on Lie group representations for rotations, which, while mathematically elegant, require a deep understanding of differential geometry. This limits accessibility for engineers and practitioners unfamiliar with these advanced mathematical concepts. A coordinate-based formulation would be more approachable and widely applicable in engineering practice.

1.2 Contributions

To bridge these gaps, our work contributes to the field in the following key areas:

C1) We propose a novel, infinite-dimensional PH formulation for planar GEBs, which naturally accommodates large deformations and rotations while ensuring intrinsic energy consistency. This formulation allows for seamless interconnection with other PH systems.

C2) We analyze the structure-preserving spatial and temporal discretization using mixed finite elements and second-order time-stepping methods. Our approach yields a new energy-momentum (EM) scheme and thus ensures exact discrete representations of the energy and angular momentum balance, enhancing long-term simulation accuracy.

C3) We demonstrate that the mixed finite element approach, naturally induced by the PH framework, mitigates shear locking for planar GEBs.

In our previous work, we applied an analogous PH-based approach to geometrically exact strings [24] and incorporated energy-consistent dissipation models [25]. Therein, the specific PH framework [42–45] has been proven useful also in the finite-dimensional setting. Here, we adopt this formulation for planar beams, addressing the specific challenges associated with their nonlinear geometry and deformation behavior.

1.3 Assumptions

We exclusively consider planar problems here to avoid additional challenges related to the parametrization of spatial rotations. For simplicity, we also assume the cross-section as well as material parameters of the beam to be constant along its centerline. Although the kinematical description is entirely nonlinear in this work, thus allowing large rotations and displacements, it is sensible to locally assume small deformations. To this end, we restrict ourselves to a linear St. Venant-Kirchhoff type stress-strain relation at some point throughout the discretization procedure. Nevertheless, nonlinear constitutive laws may be included in a straightforward manner, effecting only the necessary time discretization. Analogously to the previous works [24, 25] one could exemplarily use discrete gradients to obtain EM schemes in that case.

1.4 Notation

Vector-valued functions are denoted using bold faces, e.g. $\mathbf{a}, \mathbf{b} \in \mathbb{R}^2$. Scalars assume italic fonts, e.g. $c, d \in \mathbb{R}$. Moreover, we write $\mathbf{a} = \sum_{\alpha=1}^2 a_\alpha \mathbf{e}_\alpha$, where $\mathbf{e}_\alpha$ denotes a unit vector of a Euclidean inertial frame in $\mathbb{R}^2$. The scalar product of two vector-valued quantities is denoted by means of the dot product, e.g. $\mathbf{a} \cdot \mathbf{b} = \mathbf{a}^\top \mathbf{b} = a_1 b_1 + a_2 b_2$. We define the result of a cross-product of two vectors from $\mathbb{R}^2$ as $c = \mathbf{a} \times \mathbf{b} = a_1 b_2 - a_2 b_1$. For simplicity we introduce a representation using a constant, skew-symmetric matrix $\mathbf{S} \in \mathbb{R}^{2 \times 2}$ such that

$$\mathbf{a} \times \mathbf{b} = \mathbf{a}^\top \mathbf{S} \mathbf{b} = (\mathbf{S}^\top \mathbf{a}) \cdot \mathbf{b}, \quad \text{where} \quad \mathbf{S} := \begin{bmatrix} 0 & 1 \\ -1 & 0 \end{bmatrix}. \tag{1}$$

Partial derivatives of sufficiently smooth vector functions are denoted by $\partial_s \mathbf{n}(s, t) = \partial \mathbf{n}(s, t)/\partial s$. Second partial derivatives are written as, e.g., $\partial_s^2 \mathbf{n}(s, t) = \partial^2 \mathbf{n}(s, t)/\partial s^2$ or $\partial_{st}^2 \mathbf{n}(s, t) = \partial^2 \mathbf{n}(s, t)/\partial s \partial t$. For the inner product over a one-dimensional domain parameterized by an arc-length coordinate s, we denote

$$(\mathbf{a}, \mathbf{b})_\Omega := \int_\Omega \mathbf{a} \cdot \mathbf{b} \, \mathrm{d}s, \quad (c, d)_\Omega := \int_\Omega c \, d \, \mathrm{d}s, \tag{2}$$
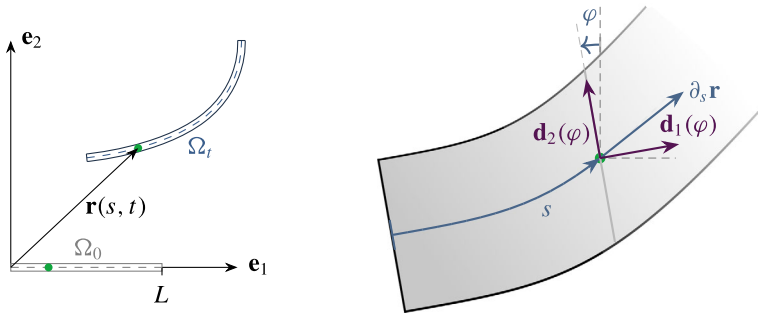
Fig. 1 Geometrically exact beam kinematics

always taking into account the dimension of the respective quantities. Identity matrices are denoted by $\mathbf{I}$ and matrices full of zeros by $\mathbf{0}$, their dimension being clear from the context. The square $\square$ represents a placeholder and will be used for instance in differential operator matrices.

1.5 Outline

The remainder of this work is structured as follows: In Sect. 2 we introduce the initial boundary value problem (IBVP) connected to planar GEB dynamics. Section 3 starts by reformulating this IBVP as an infinite-dimensional PH system and analyzes underlying conservation principles. In Sect. 4, the structure-preserving discretization in space and time is demonstrated, also showing that discrete versions of the conservation properties can be obtained. We also show that the newly devised EM scheme distinguishes itself from previously developed EM schemes. Section 5 contains numerical results for example problems. A conclusion is given in Sect. 6. Derivations and details, which are not crucial for the bulk part of the work, are comprised in Appendices A.1-A.5.

2 Problem description

Consider a one-dimensional material beam configuration $\Omega = [0, L]$, with length $L \in \mathbb{R}$, such that the motion of each material point on the centerline (also referred to as *backbone* or *line of centroids*) is described via the position vector $\mathbf{r}(s, t) \in \Omega_t \subset \mathbb{R}^2$. Here, the independent quantities are the material (arc-length) coordinate $s \in \Omega$, which parameterizes the centerline of the stress-free and straight initial configuration $\Omega_0 = \{\mathbf{r}(s, 0) = s\mathbf{e}_1 | s \in \Omega\}$, and time $t \in [0, T] \subset \mathbb{R}$, see Fig. 1. Allowing a geometrically exact description of the kinematics, every cross-section remains planar during motion and its orientation is described by means of an angle $\varphi : \Omega \times [0, T] \to \mathbb{R}$, which parameterizes a local rotation matrix

$$\mathbf{\Lambda}(\varphi(s, t)) = \begin{bmatrix} \cos\varphi(s, t) & -\sin\varphi(s, t) \\ \sin\varphi(s, t) & \cos\varphi(s, t) \end{bmatrix} \tag{3}$$

from $SO(2)$, the special orthogonal group in two dimensions. Hence, it holds that $\mathbf{\Lambda}^\top = \mathbf{\Lambda}^{-1}$ and $\det \mathbf{\Lambda} = 1$. In the following, the explicit dependency on the spatial and temporal domains

is omitted and only mentioned where deemed necessary. It can be easily verified that the relationships

$$\partial_s \mathbf{\Lambda} = \partial_s \varphi \, \mathbf{S}^\top \mathbf{\Lambda}, \qquad \partial_t \mathbf{\Lambda} = \partial_t \varphi \, \mathbf{S}^\top \mathbf{\Lambda} \tag{4}$$

hold, where the skew-symmetric matrix $\mathbf{S}$ has been introduced in (1). To quantify the strain in the beam we use two material strain measures. The first one is given by

$$\mathbf{\Gamma} = \begin{bmatrix} \Gamma_1 \\ \Gamma_2 \end{bmatrix} = \mathbf{\Lambda}^\top \partial_s \mathbf{r} - \begin{bmatrix} 1 \\ 0 \end{bmatrix}, \tag{5}$$

where $\partial_s \mathbf{r}$ is the spatial tangent vector to the deformed centerline of the beam. Consequently, Γ_1 can be linked to a dilation and Γ_2 to the transverse shear strain. Additionally, we consider the curvature measure

$$\kappa = \partial_s \varphi, \tag{6}$$

which can be interpreted as the rate of change of orientation when moving along the beam. Note that for the straight initial configuration, relations (5) and (6) induce $\mathbf{\Gamma}(s, 0) = \mathbf{0}$ and $\kappa(s, 0) = 0$, for all $s \in \Omega$. Moreover, the rotation matrix can be expressed in terms of unit directors $\{\mathbf{d}_\alpha\}_{\alpha=1}^2$, where $\mathbf{d}_1$ is normal to each cross section and $\mathbf{d}_2$ transverse to it, such that $\mathbf{\Lambda} = [\mathbf{d}_1, \mathbf{d}_2]$. Now, the physical nature of the strain quantities can be underlined since $\Gamma_1 = \mathbf{d}_1 \cdot \partial_s \mathbf{r} - 1$ and $\Gamma_2 = \mathbf{d}_2 \cdot \partial_s \mathbf{r}$. We further remark that one may also write $\mathbf{d}_\alpha = \mathbf{\Lambda} \mathbf{e}_\alpha$, $\alpha \in \{1, 2\}$.

The kinetic energy of the beam is defined as the functional

$$\mathcal{T}(\mathbf{r}, \varphi) = \int_\Omega \left(\frac{1}{2} \rho A \partial_t \mathbf{r} \cdot \partial_t \mathbf{r} + \frac{1}{2} \rho I (\partial_t \varphi)^2 \right) \mathrm{d}s, \tag{7}$$

where the mass density per unit length is denoted as $\rho A \in \mathbb{R}_{\geq 0}$ and the rotational inertia per unit length is $\rho I \in \mathbb{R}_{\geq 0}$. Additionally, the constitutive behavior is assumed to be governed by an elastic potential that enters the total potential energy

$$\mathcal{V}(\mathbf{r}, \varphi) = \int_\Omega W(\mathbf{\Gamma}, \kappa) \, \mathrm{d}s. \tag{8}$$

Therein, W denotes the strain energy density function. The material stress resultants are defined as partial derivatives of the strain energy density, i.e.

$$\mathbf{N} = \partial_{\mathbf{\Gamma}} W \quad \text{and} \quad M = \partial_\kappa W. \tag{9}$$

Their spatial counterparts can be determined by $\mathbf{n} = \mathbf{\Lambda} \mathbf{N}$ for the spatial internal force vector and $m = M$ for the spatial internal moment. Note that $\mathbf{N}$ contains both the normal and shear force while M denotes the material bending moment.

Remark 2.1 For a linear-elastic material model, one can assume a St. Venant-Kirchhoff type quadratic potential $W(\mathbf{\Gamma}, \kappa) = \frac{1}{2} \mathbf{\Gamma}^\top \mathbf{D}_{\mathrm{ts}} \mathbf{\Gamma} + \frac{1}{2} EI\kappa^2$ with

$$\mathbf{D}_{\mathrm{ts}} = \begin{bmatrix} EA & 0 \\ 0 & kGA \end{bmatrix}. \tag{10}$$

Therein, the cross-sectional area A, the elastic modulus E, the shear modulus G and shear stiffness correction factor k appear. Correspondingly, (9) gives rise to $\mathbf{N} = \mathbf{D}_{\mathrm{ts}} \mathbf{\Gamma}$ and $M = EI\kappa$.

Using Hamilton's principle one can derive the following partial differential equations (PDEs), which can be recognized as local balance equations for angular and linear momentum [4, 5], i.e.

$$\rho A \partial_t^2 \mathbf{r}(s,t) = \partial_s(\mathbf{\Lambda N})(s,t) + \overline{\mathbf{n}}(s,t),$$
$$\rho I \partial_t^2 \varphi(s,t) = \partial_s M(s,t) + \partial_s \mathbf{r}(s,t) \times (\mathbf{\Lambda N})(s,t) + \overline{m}(s,t),$$
(11)

where external distributed forces $\overline{\mathbf{n}}$ and torques $\overline{m}$ have been introduced.

The nonlinear initial boundary value problem (IBVP) at hand is completed by possibly mixed boundary conditions on $\partial\Omega = \{0, L\} = \partial\Omega_D \cup \partial\Omega_N$, e.g.

$$\mathbf{r}(s=0,t) = \mathbf{r}_D(t), \qquad \mathbf{n}(s=L,t) = \mathbf{n}_N(t),$$
$$\varphi(s=0,t) = \varphi_D(t), \qquad m(s=L,t) = m_N(t),$$
(12)

where $\partial\Omega_D$ at $s=0$ denotes the Dirichlet boundary, $\partial\Omega_N$ refers to the Neumann boundary at $s = L$ and $(\square)_{D/N}$ indicates a prescribed quantity on the respective boundary. Lastly, appropriate initial values

$$\mathbf{r}(s,0) = \mathbf{r}_0(s) \quad \text{on} \quad \Omega,$$
$$\varphi(s,0) = \varphi_0(s) \quad \text{on} \quad \Omega,$$
(13)

with prescribed data $(\square)_0$, are required.

Eventually, the IBVP looks for solutions $(\mathbf{r}^*, \varphi^*)$ of the PDEs (11) along with the constitutive closure relations (9) such that (12) and (13) are satisfied.

3 Port-Hamiltonian formulation

We propose a PH formulation for planar geometrically exact beam dynamics and subsequently develop a structure-preserving spatial and temporal discretization approach. In a first step, this involves a reformulation of the above IBVP as outlined in the following.

3.1 Reformulation as infinite-dimensional port-Hamiltonian system

To rewrite the above IBVP (11) for geometrically exact beams as an infinite-dimensional PH system [20], we introduce an extended set of variables. Besides the state variables from the Lagrangian formulation, also the strains $(\mathbf{\Gamma}, \kappa)$ and velocities

$$\mathbf{v} := \partial_t \mathbf{r}, \qquad \omega := \partial_t \varphi$$
(14)

are introduced as independent variables. Thus, the state is now given by

$$\mathbf{x} = (\mathbf{r}, \varphi, \mathbf{v}, \omega, \mathbf{\Gamma}, \kappa).$$
(15)

The total energy, also referred to as *Hamiltonian* functional, of the beam is given by

$$\mathcal{H}(\mathbf{x}) = \int_\Omega H(\mathbf{x})\,\mathrm{d}s = \int_\Omega \left(\frac{1}{2}\rho A \mathbf{v} \cdot \mathbf{v} + \frac{1}{2}\rho I \omega^2 + W(\mathbf{\Gamma}, \kappa) \right)\mathrm{d}s,$$
(16)

being the sum of kinetic energy (7) and the internal potential energy[1] (8). Additionally, we have introduced the Hamiltonian density per unit length H in equation (16). We moreover require evolution equations for the strains, which can be deduced from their definitions (5) and (6) as well as (4), such that

$$\partial_t \mathbf{\Gamma} = \omega \mathbf{\Lambda}^\top \mathbf{S} \partial_s \mathbf{r} + \mathbf{\Lambda}^\top \partial_s \mathbf{v},$$
$$\partial_t \kappa = \partial_s \omega. \tag{17}$$

Now, it is possible to formulate the IBVP from the previous Section equivalently in terms of the extended state (15) as a set of PDEs

$$\partial_t \mathbf{r} = \mathbf{v}, \tag{18a}$$

$$\partial_t \varphi = \omega, \tag{18b}$$

$$\rho A \partial_t \mathbf{v} = \partial_s (\mathbf{\Lambda N}) + \overline{\mathbf{n}}, \tag{18c}$$

$$\rho I \partial_t \omega = \partial_s M + \partial_s \mathbf{r}^\top \mathbf{S \Lambda N} + \overline{m}, \tag{18d}$$

$$\partial_t \mathbf{\Gamma} = \omega \mathbf{\Lambda}^\top \mathbf{S} \partial_s \mathbf{r} + \mathbf{\Lambda}^\top \partial_s \mathbf{v}, \tag{18e}$$

$$\partial_t \kappa = \partial_s \omega. \tag{18f}$$

along with the constitutive closure relations (9) and appropriate initial and boundary conditions, conforming with (12) and (13).

To highlight the PH structure of the above PDEs and to show that the problem at hand is an infinite-dimensional PH system [20, 24, 42, 44], we make use of a matrix operator notation such that

$$
\begin{bmatrix} \mathbf{I} & & & & & \\ & 1 & & & & \\ & & \rho A \mathbf{I} & & & \\ & & & \rho I & & \\ & & & & \mathbf{I} & \\ & & & & & 1 \end{bmatrix} \partial_t \begin{bmatrix} \mathbf{r} \\ \varphi \\ \mathbf{v} \\ \omega \\ \mathbf{\Gamma} \\ \kappa \end{bmatrix} =
$$
$$
\begin{bmatrix} & & \mathbf{I} & & & \\ & & & 1 & & \\ -\mathbf{I} & & & & \partial_s(\mathbf{\Lambda}(\varphi)\square) & \\ & -1 & & & \partial_s \mathbf{r}^\top \mathbf{S \Lambda}(\varphi)\square & \partial_s \square \\ & & \mathbf{\Lambda}(\varphi)^\top \partial_s \square & \square \mathbf{\Lambda}(\varphi)^\top \mathbf{S} \partial_s \mathbf{r} & & \\ & & & \partial_s \square & & \end{bmatrix} \begin{bmatrix} \mathbf{0} \\ 0 \\ \mathbf{v} \\ \omega \\ \mathbf{N} \\ M \end{bmatrix} + \begin{bmatrix} \mathbf{0} & 0 \\ 0 & 0 \\ \mathbf{I} & 0 \\ 0 & 1 \\ \mathbf{0} & 0 \\ 0 & 0 \end{bmatrix} \begin{bmatrix} \overline{\mathbf{n}} \\ \overline{m} \end{bmatrix}, \tag{19}
$$

where zero-entries have been omitted to improve readability. The above equation can be written in the compact form

$$\mathcal{E} \partial_t \mathbf{x} = \mathcal{J}(\mathbf{x}) \mathbf{z}(\mathbf{x}) + \mathcal{B} \mathbf{u}, \tag{20}$$

which is a specific description of a PH system going back to Mehrmann and co-workers [42, 44], see also related works such as [24, 32, 34] for other infinite-dimensional mechanical systems. One major benefit of this specific formulation is that it may integrate constraints leading to partial differential-algebraic systems. In the PH state differential equation (20),

---

[1]Note that the potential of external loads is not included in (16). Instead, external distributed forces and torques essentially take the role of inputs acting on the system.

$\mathcal{E}$ is a symmetric and constant coefficient matrix, $\mathcal{B}$ is referred to as *control* or *input* matrix operator, which is also constant. The distributed *control input* $\mathbf{u} = (\overline{\mathbf{n}}, \overline{m})$ contains the external distributed forces and torques per unit length. We have moreover introduced the so-called *co-state* function $\mathbf{z}$ being dependent on the state $\mathbf{x}$ given by (15). The differential *structure* matrix operator $\mathcal{J}$ is *formally skew-adjoint* (see also the upcoming Sect. 3.2 and particularly Remark 3.1), and state-dependent. The state-dependency here reflects the geometric nonlinearity of the problem at hand. Corresponding to the distributed control input, power-conjugated and collocated output quantities are defined through

$$\mathbf{y} = \mathcal{B}^\top \mathbf{z}(\mathbf{x}) = \begin{bmatrix} \mathbf{v} \\ \omega \end{bmatrix}. \tag{21}$$

It is known that (20) enjoys a PH structure, if and only if

$$\mathcal{E}^\top \mathbf{z}(\mathbf{x}) = \delta_{\mathbf{x}} \mathcal{H}(\mathbf{x}), \tag{22}$$

where $\delta_{\mathbf{x}} H$ represent the variational derivative of the Hamiltonian functional. In the present case, the Hamiltonian density H does not depend on derivatives of the state. Accordingly, one obtains

$$\delta_{\mathbf{x}} \mathcal{H}(\mathbf{x}) = \partial_{\mathbf{x}} H(\mathbf{x}) = (\mathbf{0}, 0, \rho A \mathbf{v}, \rho I \omega, \partial_{\Gamma} W, \partial_{\kappa} W), \tag{23}$$

such that (22) holds true in view of the constitutive laws (9).

3.2 Energy balance and passivity

The formal skew-adjointness of $\mathcal{J}$ is crucial for the energy balance, which in general takes into account the power transmitted into the system across its boundary. To see this, we consider

$$\partial_t \mathcal{H} = (\delta_{\mathbf{x}} \mathcal{H}, \partial_t \mathbf{x})_\Omega = \left(\mathcal{E}^\top \mathbf{z}, \partial_t \mathbf{x} \right)_\Omega = (\mathbf{z}, \mathcal{E} \partial_t \mathbf{x})_\Omega = (\mathbf{z}, \mathcal{J} \mathbf{z})_\Omega + (\mathbf{z}, \mathcal{B} \mathbf{u})_\Omega, \tag{24}$$

where we have subsequently inserted (22) and (20). After a straightforward calculation, the first term on the right-hand side of the last equation yields

$$
\begin{aligned}
(\mathbf{z}, \mathcal{J} \mathbf{z})_\Omega = {} & (\mathbf{v}, \partial_s \mathbf{n})_\Omega + (\mathbf{n}, \partial_s \mathbf{v})_\Omega + (\omega, \partial_s M)_\Omega + (M, \partial_s \omega)_\Omega \\
& + (\partial_s \mathbf{r}, \omega \mathbf{S} \mathbf{n})_\Omega + (\mathbf{n}, \omega \mathbf{S} \partial_s \mathbf{r})_\Omega.
\end{aligned}
\tag{25}
$$

Integration by parts implies the following relationships

$$
\begin{aligned}
(\mathbf{v}, \partial_s \mathbf{n})_\Omega &= - (\mathbf{n}, \partial_s \mathbf{v})_\Omega + [\mathbf{v} \cdot \mathbf{n}]_{\partial \Omega}, \\
(\omega, \partial_s M)_\Omega &= - (M, \partial_s \omega)_\Omega + [\omega M]_{\partial \Omega}.
\end{aligned}
\tag{26}
$$

Inserting from (26) into (25) and canceling out the last two terms in (25) due to the skew-symmetry of $\mathbf{S}$ yields

$$(\mathbf{z}, \mathcal{J} \mathbf{z})_\Omega = [\mathbf{v} \cdot \mathbf{n}]_{\partial \Omega} + [\omega M]_{\partial \Omega}. \tag{27}$$

Moreover, the second term on the right-hand side of (24) can be recast in the form

$$(\mathbf{z}, \mathcal{B} \mathbf{u})_\Omega = \left(\mathbf{u}, \mathcal{B}^\top \mathbf{z} \right)_\Omega = (\mathbf{u}, \mathbf{y})_\Omega, \tag{28}$$

where definition (21) of the output $\mathbf{y}$ has been taken into account. Thus, (24) can eventually be written as

$$\partial_t \mathcal{H} = [\mathbf{v} \cdot \mathbf{n}]_{\partial\Omega} + [\omega M]_{\partial\Omega} + (\mathbf{u}, \mathbf{y})_\Omega. \tag{29}$$

The last equation complies with the balance law for energy. In particular, the boundary terms on the right-hand side account for the power transmitted across the boundary of the system. Depending on the specific boundary conditions, (29) can be recast in the form

$$\partial_t \mathcal{H} = \mathbf{u}_\partial \cdot \mathbf{y}_\partial + (\mathbf{u}, \mathbf{y})_\Omega, \tag{30}$$

where $(\mathbf{u}_\partial, \mathbf{y}_\partial)$ is the boundary input-output pair. For example, in the case of the mixed boundary conditions (12), one has

$$\mathbf{u}_\partial = \begin{bmatrix} \mathbf{v}_\mathrm{D}(t) \\ \omega_\mathrm{D}(t) \\ \mathbf{n}_\mathrm{N}(t) \\ m_\mathrm{N}(t) \end{bmatrix} \text{ and } \mathbf{y}_\partial = \begin{bmatrix} -\mathbf{n}(0, t) \\ -m(0, t) \\ \mathbf{v}(L, t) \\ \omega(L, t) \end{bmatrix}. \tag{31}$$

Note that the balance law for energy (30) automatically ensures conservation of energy for closed systems (i.e. for $\mathbf{u} = \mathbf{0}$, $\mathbf{u}_\partial = \mathbf{0}$) and demonstrates the property of passivity. This property lies at the core of PH systems and can be exploited for advanced control design. Later, when it comes to the numerical discretization, we aim to preserve the PH structure to retain this property in simulations.

Remark 3.1 The property of formal skew-adjointness is basically an extension of skew-symmetry for matrices to differential matrix operators. Loosely speaking, this means that the computation of $(\mathbf{z}, \mathcal{J}\mathbf{z})_\Omega$ may only yield boundary terms after integration by parts, see (27). This property can be briefly written as $\mathcal{J} = -\mathcal{J}^*$. For more details, see e.g. [41] or Ch. 4 in [19].

Remark 3.2 The underlying mathematical notion is that of a Stokes-Dirac structure, which defines so-called *flow* and *effort* variables on respective dual spaces. This Stokes-Dirac structure is modulated by the state, which can be seen from the state-dependency of the structure matrix operator $\mathcal{J}(\mathbf{x})$. For more detailed explanations on this topic, the interested reader is referred to Ch. 4 in [19], or related works like [26, 34] or [41].

Remark 3.3 Dissipative material behavior can be easily incorporated into the formulation, as e.g. already demonstrated in [25]. Eventually, the PH differential equations are modified such that

$$\mathcal{E}\partial_t \mathbf{x} = (\mathcal{J}(\mathbf{x}) - \mathcal{R}(\mathbf{x}))\,\mathbf{z}(\mathbf{x}) + \mathcal{B}\mathbf{u}, \tag{32}$$

where $\mathcal{R} = \mathcal{R}^*$ is a self-adjoint, positive semi-definite dissipation matrix operator containing dissipative terms. The PH system remains passive and moreover exhibits dissipation, i.e.

$$\partial_t \mathcal{H} = (\delta_\mathbf{x} \mathcal{H}(\mathbf{x}), \partial_t \mathbf{x})_\Omega = (\mathbf{z}, \mathcal{J}(\mathbf{x})\mathbf{z})_\Omega - (\mathbf{z}, \mathcal{R}\mathbf{z})_\Omega + (\mathbf{u}, \mathbf{y})_\Omega$$
$$\leq \mathbf{u}_\partial \cdot \mathbf{y}_\partial + (\mathbf{u}, \mathbf{y})_\Omega \tag{33}$$

since $(\mathbf{z}, \mathcal{R}\mathbf{z})_\Omega \geq 0$ for all $\mathbf{z}$.

3.3 Weak formulation

The weak form of the IBVP can be derived in a straightforward manner from the differential form. Accordingly, pre-multiplying (19) on both sides by appropriate test functions $(\mathbf{w_r}, w_\varphi, \mathbf{w_v}, w_\omega, \mathbf{w_\Gamma}, w_\kappa)$, integrating over the spatial domain Ω and applying integration by parts yields

$$(\mathbf{w_r}, \partial_t \mathbf{r} - \mathbf{v})_\Omega = 0, \qquad (34a)$$

$$\left(w_\varphi, \partial_t \varphi - \omega\right)_\Omega = 0, \qquad (34b)$$

$$(\mathbf{w_v}, \rho A \partial_t \mathbf{v})_\Omega + (\partial_s(\mathbf{w_v}), \mathbf{\Lambda N})_\Omega - [\mathbf{w_v} \cdot \mathbf{n_N}]_{\partial \Omega_N} - (\mathbf{w_v}, \overline{\mathbf{n}})_\Omega = 0, \qquad (34c)$$

$$(w_\omega, \rho I \partial_t \omega)_\Omega + (\partial_s(w_\omega), M)_\Omega - \left(w_\omega, \partial_s \mathbf{r}^\top \mathbf{S \Lambda N}\right)_\Omega - [w_\omega m_N]_{\partial \Omega_N} - (w_\omega, \overline{m})_\Omega = 0, \qquad (34d)$$

$$(\mathbf{w_\Gamma}, \partial_t \mathbf{\Gamma})_\Omega - \left(\mathbf{w_\Gamma}, \omega \mathbf{\Lambda}^\top \mathbf{S} \partial_s \mathbf{r}\right)_\Omega - \left(\mathbf{w_\Gamma}, \mathbf{\Lambda}^\top \partial_s \mathbf{v}\right)_\Omega = 0, \qquad (34e)$$

$$(w_\kappa, \partial_t \kappa - \partial_s \omega)_\Omega = 0, \qquad (34f)$$

for all sufficiently smooth test functions. To obtain (34c) and (34d) vanishing test functions on the Dirichlet boundary have been taken into account. Note that the constitutive relations (9) will be required in a weak sense as well. Correspondingly, we write

$$(\mathbf{w_N}, \mathbf{N} - \partial_\Gamma W)_\Omega = 0, \qquad (34g)$$

$$(w_M, M - \partial_\kappa W)_\Omega = 0, \qquad (34h)$$

introducing additional test functions $\mathbf{w_N}$ and w_M.

Remark 3.4 The weak form (34a)–(34h) is valid if the Dirichlet boundary conditions are considered in the space of admissible test functions. However, if the Dirichlet boundary conditions are to be enforced in a weak sense, the weak form must be slightly modified, e.g. by introducing additional Lagrange multipliers and accounting for the prescribed boundary values. In general, enforcing non-homogeneous mixed boundary conditions for PH systems requires additional care, see, for example, [23, 46–48].

Remark 3.5 The inclusion of the constitutive laws in the weak form (34a)–(34h) may appear unconventional at first. However, this will be handy later on in the structure-preserving discretization procedure. Additionally, this highlights the close connection of the present weak form with a 8-field Hu-Washizu-like variational principle $\delta S_{HW}(\mathbf{r}, \varphi, \mathbf{v}, \omega, \mathbf{\Gamma}, \kappa, \mathbf{N}, M) = 0$. To this end, choose the test functions as

$$\begin{aligned} \mathbf{w_r} &= \rho A \delta \mathbf{v}, & w_\varphi &= \rho I \delta \omega, & \mathbf{w_v} &= \delta \mathbf{r}, & w_\omega &= \delta \varphi, \\ \mathbf{w_\Gamma} &= \delta \mathbf{N}, & w_\kappa &= \delta M, & \mathbf{w_N} &= \delta \mathbf{\Gamma}, & w_M &= \delta \kappa. \end{aligned} \qquad (35)$$

Furthermore, instead of the rate form of the strain-displacement relationships in (34e) and (34f), the variational principle yields the strain-displacement relationships (5) and (6). For the details, see Appendix A.1.

3.4 Balance of total angular momentum

The total angular momentum of the planar beam relative to the origin of the coordinate frame is defined by

$$J = \int_\Omega \left(\mathbf{r}^\top \mathbf{S} \rho A \mathbf{v} + \rho I \omega \right) \, \mathrm{d}s. \tag{36}$$

Assuming a pure Neumann problem (i.e. no Dirichlet boundary conditions), the following choice of admissible test functions

$$\mathbf{w_r} = \mathbf{S}^\top \rho A \mathbf{v}, \quad \mathbf{w_v} = \mathbf{S}^\top \mathbf{r}, \quad \text{and} \quad w_\omega = 1, \tag{37}$$

can be made in the weak form (34a)–(34h). Accordingly, inserting these functions into (34a), (34c) and (34d) and subsequently adding the resulting equations yields

$$\begin{aligned}
\left(\mathbf{S}^\top \rho A \mathbf{v}, \partial_t \mathbf{r} \right)_\Omega + \left(\mathbf{S}^\top \mathbf{r}, \rho A \partial_t \mathbf{v} \right)_\Omega + \left(1, \rho I \partial_t \omega \right)_\Omega = & \\
\left(\mathbf{S}^\top \rho A \mathbf{v}, \mathbf{v} \right)_\Omega - \left(\partial_s (\mathbf{S}^\top \mathbf{r}), \mathbf{\Lambda N} \right)_\Omega + \left[\mathbf{S}^\top \mathbf{r} \cdot \mathbf{n}_\mathrm{N} \right]_{\partial \Omega_\mathrm{N}} + \left(\mathbf{S}^\top \mathbf{r}, \overline{\mathbf{n}} \right)_\Omega & \\
+ \left(1, \partial_s \mathbf{r}^\top \mathbf{S \Lambda N} \right)_\Omega + [m_\mathrm{N}]_{\partial \Omega_\mathrm{N}} + \left(1, \overline{m} \right)_\Omega. &
\end{aligned} \tag{38}$$

While the first term on the right-hand side of the last equation vanishes due to the skew-symmetry of matrix $\mathbf{S}$, it can be shown that the second and fifth term cancel each other. Moreover, the left-hand side can be identified as the temporal derivative of the total angular momentum (36). Thus, we arrive at the balance equation

$$\partial_t J = \int_\Omega \left(\mathbf{r}^\top \mathbf{S} \overline{\mathbf{n}} + \overline{m} \right) \, \mathrm{d}s + \left[\mathbf{r}^\top \mathbf{S} \mathbf{n}_\mathrm{N} + m_\mathrm{N} \right]_{\partial \Omega_\mathrm{N}}. \tag{39}$$

This demonstrates that the time rate of change of the total angular momentum is equal to the angular momentum exerted on the system by distributed input forces and torques as well as Neumann boundary conditions. In the special case of closed systems, the total angular momentum is preserved.

Remark 3.6 Note that the balance equation for the total energy can also be proven by employing a similar approach. In particular, choosing $\mathbf{w_v} = \mathbf{v}$, $w_\omega = \omega$, $\mathbf{w_\Gamma} = \mathbf{N}$ and $w_\kappa = M$ in weak form (34a)–(34h), subsequently adding the equations resulting from (34c)-(34f), and taking into account (34g) and (34h) with $\mathbf{w_N} = \partial_t \mathbf{\Gamma}$ and $w_M = \partial_t \kappa$, one arrives at relation (30).

4 Numerical discretization

The numerical discretization of the PH system is based on the structure-preserving mixed finite element method and energy-consistent time-stepping schemes. Crucial properties of the infinite-dimensional PH system can be carried over to the discrete setting. The methodology is summarized in the following sections.

Fig. 2 Degrees of freedom of one finite element
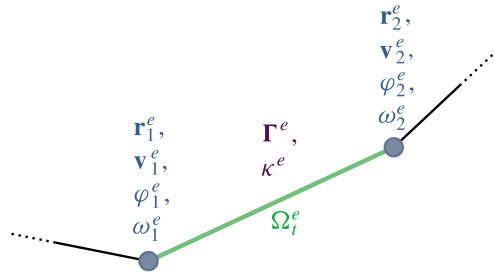
4.1 Structure-preserving spatial discretization

The PH system for the geometrically exact beam dynamics (19) is readily available for spatial discretization via its weak form (34a)–(34h). Specifically, we employ a mixed finite element approach, similar to [24, 25] and divide the beam domain into n_e finite elements, i.e. $\Omega = \cup_{e=1}^{n_e} \Omega^e$. Since we make use of 2-node finite elements (see Fig. 2), the total amount of nodes is $n_n = n_e + 1$. Displacement and velocity quantities $(\mathbf{r}, \varphi, \mathbf{v}, \omega)$ are approximated with C^0-continuous, piecewise linear Lagrangian shape functions, while strain and stress type quantities $(\mathbf{\Gamma}, \kappa, \mathbf{N}, M)$ use piecewise constant discontinuous approximations. We denote by

$$\mathcal{V}^h \subset H^1(\Omega; \mathbb{R}^2), \quad \mathcal{W}^h \subset H^1(\Omega; \mathbb{R}), \quad \mathcal{G}^h \subset L^2(\Omega; \mathbb{R}^2), \quad \mathcal{K}^h \subset L^2(\Omega; \mathbb{R}), \quad (40)$$

finite-dimensional subspaces of the Sobolev spaces of square-integrable C^0-continuous functions and of the spaces of square-integrable, piecewise constant functions. Choosing a specific basis within the Bubnov-Galerkin method, the approximation is expressed as

$$
\begin{aligned}
\mathbf{r}^h(s, t) &= \mathbf{\Phi}_2(s)\hat{\mathbf{r}}(t) \in \mathcal{V}^h, & \mathbf{v}^h(s, t) &= \mathbf{\Phi}_2(s)\hat{\mathbf{v}}(t) \in \mathcal{V}^h, \\
\varphi^h(s, t) &= \mathbf{\Phi}_1(s)\hat{\boldsymbol{\varphi}}(t) \in \mathcal{W}^h, & \omega^h(s, t) &= \mathbf{\Phi}_1(s)\hat{\boldsymbol{\omega}}(t) \in \mathcal{W}^h, \\
\mathbf{\Gamma}^h(s, t) &= \mathbf{\Psi}_2(s)\hat{\mathbf{\Gamma}}(t) \in \mathcal{G}^h, & \mathbf{N}^h(s, t) &= \mathbf{\Psi}_2(s)\hat{\mathbf{N}}(t) \in \mathcal{G}^h, \\
\kappa^h(s, t) &= \mathbf{\Psi}_1(s)\hat{\boldsymbol{\kappa}}(t) \in \mathcal{K}^h, & M^h(s, t) &= \mathbf{\Psi}_1(s)\hat{\mathbf{M}}(t) \in \mathcal{K}^h,
\end{aligned}
\tag{41}
$$

where $\square^h$ denotes an approximation of the field quantity $\square$ and the nodal-unknown vector $\hat{\square}$ contains entries from all finite elements and the respective nodes. Moreover, for the approximation of the corresponding test function $\mathbf{w}_{\square}^h$ consider the same basis as for $\square^h$. In this context, the above ansatz matrices contain the linear Lagrangian shape functions or the piecewise constant functions, e.g.

$$\mathbf{r}^h(s, t) = \mathbf{\Phi}_2(s)\hat{\mathbf{r}}(t) = \sum_{i=1}^{n_n} N_i(s)\mathbf{r}_i(t), \tag{42a}$$

$$\mathbf{\Gamma}^h(s, t) = \mathbf{\Psi}_2(s)\hat{\mathbf{\Gamma}}(t) = \sum_{i=1}^{n_e} \tilde{N}_i(s)\mathbf{\Gamma}_i(t), \tag{42b}$$

for more details see Appendix A.2. The basis functions are depicted in Fig. 3. We follow common finite element procedures, see e.g. [49, 50], which also includes an assembly of the global system matrices and vectors accounting for the respective nodal indices and degrees
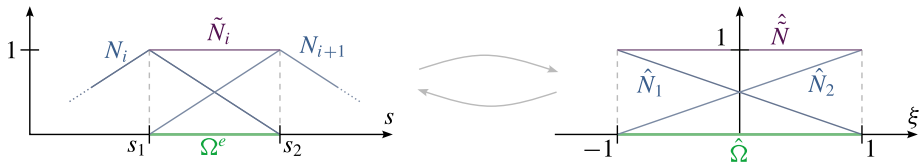
Fig. 3 Ansatz functions and reference element

of freedom, such that e.g. $\mathbf{r}_2^{e+1} = \mathbf{r}_1^e$ are the same degree of freedom. The degrees of freedom of one finite element are depicted in Fig. 2. Additionally, we perform all computations on element level and consider the isoparametric concept to transform all calculations to a standard reference element with $\xi \in \hat{\Omega} = [-1, 1]$, see Fig. 3.

Eventually, the finite-dimensional version of the state (15) contains the degrees of freedom of all finite elements and is given by

$$\hat{\mathbf{x}} = (\hat{\mathbf{r}}, \hat{\boldsymbol{\varphi}}, \hat{\mathbf{v}}, \hat{\boldsymbol{\omega}}, \hat{\boldsymbol{\Gamma}}, \hat{\boldsymbol{\kappa}}). \tag{43}$$

Inserting the ansatz (41) into (16) gives rise to the approximated Hamiltonian. Note that we henceforth assume linear-elastic constitutive relations (see Remark 2.1) for the ease of notation. The discrete Hamiltonian reads

$$\hat{\mathcal{H}}(\hat{\mathbf{x}}) = \frac{1}{2}\hat{\mathbf{v}}^\top \rho A \mathbf{M}_2 \hat{\mathbf{v}} + \frac{1}{2}\hat{\boldsymbol{\omega}}^\top \rho I \mathbf{M}_1 \hat{\boldsymbol{\omega}} + \frac{1}{2}\hat{\boldsymbol{\Gamma}}^\top \mathbf{D}_2 \hat{\boldsymbol{\Gamma}} + \frac{1}{2}\hat{\boldsymbol{\kappa}}^\top \mathbf{D}_1 \hat{\boldsymbol{\kappa}}, \tag{44}$$

where the system matrices can be found in Appendix A.3. The corresponding discrete system dynamics are obtained by approximating the weak form (34a)–(34h) with the ansatz spaces (40). The discrete system dynamics are given by

$$\left(\mathbf{w_r}^{\mathrm{h}}, \partial_t \mathbf{r}^{\mathrm{h}} - \mathbf{v}^{\mathrm{h}}\right)_\Omega = 0, \tag{45a}$$

$$\left(w_\varphi^{\mathrm{h}}, \partial_t \varphi^{\mathrm{h}} - \omega^{\mathrm{h}}\right)_\Omega = 0, \tag{45b}$$

$$\left(\mathbf{w_v}^{\mathrm{h}}, \rho A \partial_t \mathbf{v}^{\mathrm{h}}\right)_\Omega + \left(\partial_s(\mathbf{w_v}^{\mathrm{h}}), \boldsymbol{\Lambda}(\varphi^{\mathrm{h}})\mathbf{N}^{\mathrm{h}}\right)_\Omega - \left[\mathbf{w_v}^{\mathrm{h}} \cdot \mathbf{n_N}\right]_{\partial\Omega_{\mathrm{N}}} - \left(\mathbf{w_v}^{\mathrm{h}}, \overline{\mathbf{n}}\right)_\Omega = 0, \tag{45c}$$

$$\left(w_\omega^{\mathrm{h}}, \rho I \partial_t \omega^{\mathrm{h}}\right)_\Omega + \left(\partial_s(w_\omega^{\mathrm{h}}), M^{\mathrm{h}}\right)_\Omega - \left(w_\omega^{\mathrm{h}}, (\partial_s \mathbf{r}^{\mathrm{h}})^\top \mathbf{S}\boldsymbol{\Lambda}(\varphi^{\mathrm{h}})\mathbf{N}^{\mathrm{h}}\right)_\Omega - \left[w_\omega^{\mathrm{h}} m_{\mathrm{N}}\right]_{\partial\Omega_{\mathrm{N}}} - \left(w_\omega^{\mathrm{h}}, \overline{m}\right)_\Omega = 0, \tag{45d}$$

$$\left(\mathbf{w_\Gamma}^{\mathrm{h}}, \partial_t \boldsymbol{\Gamma}^{\mathrm{h}}\right)_\Omega - \left(\mathbf{w_\Gamma}^{\mathrm{h}}, \omega^{\mathrm{h}} \boldsymbol{\Lambda}(\varphi^{\mathrm{h}})^\top \mathbf{S}\partial_s \mathbf{r}^{\mathrm{h}}\right)_\Omega - \left(\mathbf{w_\Gamma}^{\mathrm{h}}, \boldsymbol{\Lambda}(\varphi^{\mathrm{h}})^\top \partial_s \mathbf{v}^{\mathrm{h}}\right)_\Omega = 0, \tag{45e}$$

$$\left(w_\kappa^{\mathrm{h}}, \partial_t \kappa^{\mathrm{h}} - \partial_s \omega^{\mathrm{h}}\right)_\Omega = 0, \tag{45f}$$

$$\left(\mathbf{w_N}^{\mathrm{h}}, \mathbf{N}^{\mathrm{h}} - \mathbf{D}_{\mathrm{ts}}\boldsymbol{\Gamma}^{\mathrm{h}}\right)_\Omega = 0, \tag{45g}$$

$$\left(w_M^{\mathrm{h}}, M^{\mathrm{h}} - EI\kappa^{\mathrm{h}}\right)_\Omega = 0. \tag{45h}$$

With the chosen basis functions from (41) it is possible to transform the above variational formulation into a finite-dimensional PH system in terms of differential equations, assuming the arbitrariness of the test functions. We arrive at the discrete PH system governed by

$$
\begin{bmatrix}
\mathbf{M}_2 & & & & & \\
& \mathbf{M}_1 & & & & \\
& & \rho A\mathbf{M}_2 & & & \\
& & & \rho I\mathbf{M}_1 & & \\
& & & & \mathbf{C}_2 & \\
& & & & & \mathbf{C}_1
\end{bmatrix}
\frac{\mathrm{d}}{\mathrm{d}t}
\begin{bmatrix}
\hat{\mathbf{r}} \\
\hat{\boldsymbol{\varphi}} \\
\hat{\mathbf{v}} \\
\hat{\boldsymbol{\omega}} \\
\hat{\boldsymbol{\Gamma}} \\
\hat{\boldsymbol{\kappa}}
\end{bmatrix}
=
\tag{46}
$$

$$
\begin{bmatrix}
& & \mathbf{M}_2 & & & \\
& & & \mathbf{M}_1 & & \\
-\mathbf{M}_2^\top & & & & -\mathbf{G}_2(\hat{\boldsymbol{\varphi}}) & \\
& -\mathbf{M}_1^\top & & & \mathbf{V}(\hat{\mathbf{r}},\hat{\boldsymbol{\varphi}}) & -\mathbf{G}_1 \\
& \mathbf{G}_2(\hat{\boldsymbol{\varphi}})^\top & -\mathbf{V}(\hat{\mathbf{r}},\hat{\boldsymbol{\varphi}})^\top & & & \\
& & \mathbf{G}_1^\top & & &
\end{bmatrix}
\begin{bmatrix}
\mathbf{0} \\
\mathbf{0} \\
\hat{\mathbf{v}} \\
\hat{\boldsymbol{\omega}} \\
\hat{\mathbf{N}} \\
\hat{\mathbf{M}}
\end{bmatrix}
+
\begin{bmatrix} \mathbf{B}_\partial & \mathbf{B}_\Omega \end{bmatrix}
\begin{bmatrix}
\mathbf{u}_\partial(t) \\
\hat{\mathbf{u}}_\Omega(t)
\end{bmatrix}.
$$

along with the algebraic constraints for the stress resultants

$$
\mathbf{C}_2\hat{\mathbf{N}} = \mathbf{D}_2\hat{\boldsymbol{\Gamma}}, \quad \text{and} \quad \mathbf{C}_1\hat{\mathbf{M}} = \mathbf{D}_1\hat{\boldsymbol{\kappa}},
\tag{47}
$$

emerging from (45g) and (45h). For the detailed definitions of the system matrices see Appendix A.3. For the implementation details concerning the input vectors and matrices, which deal with both distributed and boundary inputs, we refer to Appendix A.4. Note that the system output $\hat{\mathbf{y}}$ contains both angular and translational velocities in the domain and at the boundary, i.e.

$$
\hat{\mathbf{y}} = \begin{bmatrix} \mathbf{y}_\partial \\ \hat{\mathbf{y}}_\Omega \end{bmatrix} = \begin{bmatrix} \mathbf{B}_\partial^\top \\ \mathbf{B}_\Omega^\top \end{bmatrix} \hat{\mathbf{z}}(\hat{\mathbf{x}}),
\tag{48}
$$

see also the definition in the continuous setting (31). Analogously to the infinite-dimensional version (20), we can recast the semi-discrete set of equations in the spirit of a PH framework as in [42–44] given by

$$
\mathbf{E}\frac{\mathrm{d}}{\mathrm{d}t}\hat{\mathbf{x}} = \mathbf{J}(\hat{\mathbf{x}})\hat{\mathbf{z}}(\hat{\mathbf{x}}) + \mathbf{B}\hat{\mathbf{u}},
$$
$$
\hat{\mathbf{y}} = \mathbf{B}^\top\hat{\mathbf{z}}(\hat{\mathbf{x}}),
\tag{49}
$$

where the output equation has been appended. Analogously to (20), $\mathbf{E}$ is a symmetric coefficient matrix and $\mathbf{J}(\hat{\mathbf{x}}) = -\mathbf{J}(\hat{\mathbf{x}})^\top$ denotes a skew-symmetric and state-dependent structure matrix, reflecting the geometric nonlinearity of the problem at hand. As in the infinite-dimensional case, the system (49) is PH if and only if

$$
\mathbf{E}^\top\hat{\mathbf{z}}(\hat{\mathbf{x}}) = \nabla\hat{\mathcal{H}}(\hat{\mathbf{x}})
\tag{50}
$$

holds true. In view of the discrete Hamiltonian (44) this can be verified by using the discrete constitutive relations (47).

Note that the input term $\mathbf{B}\hat{\mathbf{u}}$ contains both distributed and boundary input terms, i.e. distributed forces and torques as well as boundary quantities emanating from the Neumann boundary conditions. Moreover, $\hat{\mathbf{z}}$ is the discretized co-state function. As already shown in the infinite-dimensional setting, one core property of the PH formulation is that it satisfies a formalized energy balance, see (30). This property is inherited by the semi-discrete system (49) such that

$$
\frac{\mathrm{d}}{\mathrm{d}t}\hat{\mathcal{H}} = \nabla\hat{\mathcal{H}}(\hat{\mathbf{x}})^\top\frac{\mathrm{d}}{\mathrm{d}t}\hat{\mathbf{x}} = \hat{\mathbf{z}}(\hat{\mathbf{x}})^\top\mathbf{E}\frac{\mathrm{d}}{\mathrm{d}t}\hat{\mathbf{x}} = \hat{\mathbf{z}}(\hat{\mathbf{x}})^\top(\mathbf{J}(\hat{\mathbf{x}})\hat{\mathbf{z}}(\hat{\mathbf{x}}) + \mathbf{B}\hat{\mathbf{u}}) = \hat{\mathbf{u}}^\top\hat{\mathbf{y}},
\tag{51}
$$

where the skew-symmetry of the structure-matrix has been taken into account. This relation highlights the passivity of the finite-dimensional system and energy-conservation is obtained for closed system. The semi-discrete PH system (49) is the basis for the structure-preserving time discretization in the next section.

4.2 Structure-preserving time discretization

We aim at a structure-preserving time discretization of the semi-discrete PH system (49) with the equivalent variational formulation (45a)–(45h). To this end, we apply an implicit one-step scheme which is based on the implicit mid-point rule. Let $\hat{\mathbf{x}}_n \approx \hat{\mathbf{x}}(t_n)$ at time instance t_n and consider an equidistant time-grid such that $[0, T] = \cup_{n=0}^{N}[t_n, t_{n+1}]$ with N time steps of constant size $h = t_{n+1} - t_n$.

The time-stepping scheme we propose, given the PH system (49), can now be written in the form

$$
\begin{aligned}
\mathbf{E}\left(\hat{\mathbf{x}}_{n+1} - \hat{\mathbf{x}}_n\right) &= h\,\mathbf{J}(\hat{\mathbf{x}}_{n+1/2})\hat{\mathbf{z}}_{n+1/2} + h\,\mathbf{B}\hat{\mathbf{u}}_{n+1/2}, \\
\hat{\mathbf{y}}_{n+1/2} &= \mathbf{B}^{\top}\hat{\mathbf{z}}_{n+1/2},
\end{aligned}
\tag{52}
$$

for $n = 0, \ldots, N - 1$, where $\hat{\mathbf{x}}_{n+1/2} = \frac{1}{2}(\hat{\mathbf{x}}_{n+1} + \hat{\mathbf{x}}_n)$, While we assume that $\hat{\mathbf{u}}_{n+1/2}$ is the evaluation of the (possibly discontinuous) input function at $t_{n+1/2}$, this must not be necessarily the case. It could also be the evaluation at some other point within the time interval of interest or an average value. Additionally, the time-discrete co-state vector $\hat{\mathbf{z}}_{n+1/2}$ is defined through

$$
\mathbf{E}^{\top}\hat{\mathbf{z}}_{n+1/2} = \nabla\hat{\mathcal{H}}(\hat{\mathbf{x}}_{n+1/2}),
\tag{53}
$$

which can be inverted, since $\mathbf{E}$ is square and non-singular. Correspondingly, the discrete-time output $\hat{\mathbf{y}}_{n+1/2}$ is an approximation for $\hat{\mathbf{y}}(t_{n+1/2})$. For at most quadratic Hamiltonians, like here (44), the midpoint-evaluated gradient satisfies the directionality property[2]

$$
\nabla\hat{\mathcal{H}}(\hat{\mathbf{x}}_{n+1/2})^{\top}\left(\hat{\mathbf{x}}_{n+1} - \hat{\mathbf{x}}_n\right) = \hat{\mathcal{H}}(\hat{\mathbf{x}}_{n+1}) - \hat{\mathcal{H}}(\hat{\mathbf{x}}_n).
\tag{54}
$$

The structure-preserving scheme is energy-consistent and second-order accurate. It ensures an exact energy balance in discrete time, i.e. making use of directionality property (54) we obtain

$$
\begin{aligned}
\hat{\mathcal{H}}_{n+1} - \hat{\mathcal{H}}_n = (\hat{\mathbf{z}}_{n+1/2})^{\top}\mathbf{E}\left(\hat{\mathbf{x}}_{n+1} - \hat{\mathbf{x}}_n\right) &= (\hat{\mathbf{z}}_{n+1/2})^{\top}h\left(\mathbf{J}(\hat{\mathbf{x}}_{n+1/2})\hat{\mathbf{z}}_{n+1/2} + \mathbf{B}\hat{\mathbf{u}}_{n+1/2}\right) \\
&= h\,(\hat{\mathbf{u}}_{n+1/2})^{\top}\hat{\mathbf{y}}_{n+1/2},
\end{aligned}
\tag{55}
$$

where we have used the skew-symmetry of $\mathbf{J}$. This relation is a time-discrete counterpart of (51). This proves that the present time-stepping scheme exhibits passivity and losslessness (which includes energy-conservation in the case of vanishing inputs).

Remark 4.1 Note that analogously to [24, 25] discrete gradients may be employed in the case of nonlinear materials to obtain energy-consistency in that case. The application of discrete gradients ensures the directionality condition (54) to be true for all Hamiltonians.

---

[2]This property can be directly extended for more general Hamiltonians by means of discrete gradients [24, 45, 51, 52].

The time-stepping scheme governed by (52) and (53) corresponds to an approximation of the weak form (45a)–(45h) after choosing the above-mentioned basis functions. A direct discretization of this weak form in an equivalent manner yields

$$\left(\mathbf{w_r}^h, \mathbf{r}_{n+1}^h - \mathbf{r}_n^h - h\mathbf{v}_{n+1/2}^h\right)_\Omega = 0, \quad (56a)$$

$$\left(w_\varphi^h, \varphi_{n+1}^h - \varphi_n^h - h\omega_{n+1/2}^h\right)_\Omega = 0, \quad (56b)$$

$$\left(\mathbf{w_v}^h, \rho A(\mathbf{v}_{n+1}^h - \mathbf{v}_n^h)\right)_\Omega + \left(\partial_s(\mathbf{w_v}^h), h\mathbf{\Lambda}(\varphi_{n+1/2}^h)\mathbf{N}_{n+1/2}^h\right)_\Omega$$
$$-h\left[\mathbf{w_v}^h \cdot (\mathbf{n_N})_{n+1/2}\right]_{\partial\Omega_N} - h\left(\mathbf{w_v}^h, \overline{\mathbf{n}}_{n+1/2}\right)_\Omega = 0, \quad (56c)$$

$$\left(w_\omega^h, \rho I(\omega_{n+1}^h - \omega_n^h)\right)_\Omega + \left(\partial_s(w_\omega^h), hM_{n+1/2}^h\right)_\Omega$$
$$-\left(w_\omega^h, h(\partial_s\mathbf{r}_{n+1/2}^h)^\top\mathbf{S}\mathbf{\Lambda}(\varphi_{n+1/2}^h)\mathbf{N}_{n+1/2}^h\right)_\Omega$$
$$-h\left[w_\omega^h(m_N)_{n+1/2}\right]_{\partial\Omega_N} - h\left(w_\omega^h, \overline{m}_{n+1/2}\right)_\Omega = 0, \quad (56d)$$

$$\left(\mathbf{w_\Gamma}^h, \mathbf{\Gamma}_{n+1}^h - \mathbf{\Gamma}_n^h\right)_\Omega - \left(\mathbf{w_\Gamma}^h, h\omega_{n+1/2}^h\mathbf{\Lambda}(\varphi_{n+1/2})^\top\mathbf{S}\partial_s\mathbf{r}_{n+1/2}^h\right)_\Omega$$
$$- \left(\mathbf{w_\Gamma}^h, h\mathbf{\Lambda}(\varphi_{n+1/2}^h)^\top\partial_s\mathbf{v}_{n+1/2}^h\right)_\Omega = 0, \quad (56e)$$

$$\left(w_\kappa^h, \kappa_{n+1}^h - \kappa_n^h - h\partial_s\omega_{n+1/2}^h\right)_\Omega = 0, \quad (56f)$$

$$\left(\mathbf{w_N}^h, \mathbf{N}_{n+1/2}^h - \mathbf{D}_{ts}\mathbf{\Gamma}_{n+1/2}^h\right)_\Omega = 0, \quad (56g)$$

$$\left(w_M^h, M_{n+1/2}^h - EI\kappa_{n+1/2}^h\right)_\Omega = 0. \quad (56h)$$

The weak representation (56a)–(56h) also facilitates the following derivations.

4.3 Discrete balance of total angular momentum

Here, we show that the proposed discretization approach inherits the balance of angular momentum (39) in a discrete sense. To this end, one proceeds in very similar way to the continuous case, see Sect. 3.4. The discrete total angular momentum is defined as

$$J_n^h = \int_\Omega \left((\mathbf{r}_n^h)^\top\mathbf{S}\rho A\mathbf{v}_n^h + \rho I\omega_n^h\right) ds \qquad (57)$$

for $n = 0, \ldots, N$. It is then stated that the identity

$$J_{n+1}^h - J_n^h = \int_\Omega \left((\mathbf{r}_{n+1/2}^h)^\top\mathbf{S}\rho A(\mathbf{v}_{n+1}^h - \mathbf{v}_n^h) + (\mathbf{r}_{n+1}^h - \mathbf{r}_n^h)^\top\mathbf{S}\rho A\mathbf{v}_{n+1/2}^h \right.$$
$$\left. + \rho I(\omega_{n+1}^h - \omega_n^h)\right) ds \qquad (58)$$

holds true. Now, from all admissible test functions we set

$$\mathbf{w_r}^h = \mathbf{S}^\top\rho A\mathbf{v}_{n+1/2}^h, \quad \mathbf{w_v}^h = \mathbf{S}^\top\mathbf{r}_{n+1/2}^h, \quad \text{and} \quad w_\omega^h = 1, \qquad (59)$$

and add up the discrete-time weak forms (56a), (56c) and (56d). Eventually, the right-hand side of (58) can be identified in the result, such that

$$J_{n+1}^h - J_n^h = \int_\Omega \left((\mathbf{r}_{n+1/2}^h)^\top\mathbf{S}\overline{\mathbf{n}}_{n+1/2} + \overline{m}_{n+1/2}\right) ds$$
$$+ \left[(\mathbf{r}_{n+1/2}^h)^\top\mathbf{S}(\mathbf{n_N})_{n+1/2} + (m_N)_{n+1/2}\right]_{\partial\Omega_N} \qquad (60)$$

remains. Correspondingly, only terms induced by Neumann boundary conditions as well as distributed input forces and torques remain in the discrete balance of angular momentum. This shows that the proposed time-discretization scheme inherits the balance of angular momentum from the continuous setting and the total angular momentum is conserved for closed systems.

Remark 4.2 Note that the discrete-time balance equation for the total energy (55) can be proven alternatively by employing a similar approach with appropriate discrete-time test functions.

4.4 Comparison with the usual approach to the design of EM methods

The present PH approach to the design of EM schemes can be distinguished from previously proposed EM methods, which typically impose the strain-displacement relationships (5) and (6) at the end of each time step. In particular, the present approach relies on the time discretization of the rate form of the strain-displacement relationship (17), which is further analyzed in Sect. 4.4.1. This crucial difference is illustrated in Sect. 4.4.2 by comparing the present formulation with the classical work by Stander and Stein [39]. Lastly, we deduce a purely displacement-based version of the PH scheme making use of an internal history variable in Sect. 4.4.3. In what follows, we can focus on the temporal discretization while leaving the spatial discretization apart for the sake of conciseness.

4.4.1 Strain-displacement relationships in the time-discrete setting

Second-order EM schemes are commonly based on the application of the mid-point rule to the kinematic displacement-velocity equations. That is, in the present case of the planar beam[3]

$$\mathbf{r}_{n+1} - \mathbf{r}_n = h\mathbf{v}_{n+1/2}, \tag{61a}$$

$$\varphi_{n+1} - \varphi_n = h\omega_{n+1/2}, \tag{61b}$$

which conforms with (56a) and (56b), respectively. Our PH approach relies on the discretization of the rate form of the strain-displacement relationship (17). Accordingly, application of the mid-point rule yields

$$\mathbf{\Gamma}_{n+1} - \mathbf{\Gamma}_n = h\omega_{n+1/2}\mathbf{\Lambda}(\varphi_{n+1/2})^\top \mathbf{S}\,\partial_s \mathbf{r}_{n+1/2} + h\mathbf{\Lambda}(\varphi_{n+1/2})^\top \partial_s \mathbf{v}_{n+1/2}, \tag{62a}$$

$$\kappa_{n+1} - \kappa_n = h\partial_s \omega_{n+1/2}, \tag{62b}$$

which complies with (56e) and (56f), respectively. Substituting (61b) into (62b) yields

$$\kappa_{n+1} - \kappa_n = \partial_s \varphi_{n+1} - \partial_s \varphi_n, \tag{63}$$

which implies $\kappa_{n+1} = \partial_s \varphi_{n+1}$, since $\kappa_n = \partial_s \varphi_n$ is given for consistent initial conditions. However, a similar result is not obtained from (62a) due to the nonlinearity of the strain-displacement relation (5), i.e. $\mathbf{\Gamma} = \mathbf{\Lambda}(\varphi)^\top \partial_s \mathbf{r} - \mathbf{e}_1$. Instead, (62a) can be recast in the form

$$\mathbf{\Gamma}_{n+1} = \mathbf{\Gamma}_n + \Delta\varphi \mathbf{\Lambda}(\varphi_{n+1/2})^\top \mathbf{S}\,\partial_s \mathbf{r}_{n+1/2} + \mathbf{\Lambda}(\varphi_{n+1/2})^\top \partial_s(\Delta\mathbf{r}), \tag{64}$$

---

[3]The energy-consistent time discretization proposed in [40] for the present planar beam model is an exceptional case which relies on a modification of (61b) leading to $2\tan\frac{\varphi_{n+1}-\varphi_n}{2} = h\omega_{n+1/2}$.

where use has been made of (61a)–(61b) along with the notation

$$\Delta\varphi := \varphi_{n+1} - \varphi_n \quad \text{and} \quad \Delta\mathbf{r} := \mathbf{r}_{n+1} - \mathbf{r}_n. \tag{65}$$

Thus (64) serves as update formula for the determination of $\boldsymbol{\Gamma}_{n+1}$. Note that this is in sharp contrast to evaluating the strain-displacement relation (5) at t_{n+1}.

4.4.2 Link to the classical EM scheme by Stander & Stein

To link the present PH EM scheme to the classical EM scheme by Stander & Stein [39], we first provide a modification of (64) which enforces the fulfillment of the strain-displacement relation (5) at t_{n+1}. This is, as stated above, a typical feature of common EM methods. Accordingly, we consider the modified mid-point rule

$$\boldsymbol{\Gamma}_{n+1} - \boldsymbol{\Gamma}_n = h Z_2(\Delta\varphi)\omega_{n+1/2}\boldsymbol{\Lambda}(\varphi_{n+1/2})^\top \mathbf{S}\,\partial_s\mathbf{r}_{n+1/2} + h Z_1(\Delta\varphi)\boldsymbol{\Lambda}(\varphi_{n+1/2})^\top \partial_s\mathbf{v}_{n+1/2}, \tag{66}$$

where

$$Z_1(\Delta\varphi) := \cos\frac{\Delta\varphi}{2} \quad \text{and} \quad Z_2(\Delta\varphi) := \frac{\sin\frac{\Delta\varphi}{2}}{\frac{\Delta\varphi}{2}} \tag{67}$$

have been introduced. Since both $Z_1 \to 1$ and $Z_2 \to 1$ for $\Delta\varphi \to 0$, the consistency of the mid-point rule is not affected. Moreover, since Z_1 and Z_2 merely cause a second-order perturbation of the mid-point rule, the accuracy of the integration rule is not affected. This modification eventually yields an endpoint satisfaction of the kinematic relation such that $\boldsymbol{\Gamma}_{n+1} = \boldsymbol{\Lambda}(\varphi_{n+1})^\top \partial_s\mathbf{r}_{n+1} - \mathbf{e}_1$. For the detailed derivations, see Appendix A.5.

We continue with the weak form that lies at the heart of [39]. Specifically, the weak form can be cast in the frame of the principle of virtual work leading to

$$G^{\text{dyn}} + G^{\text{int}} = G^{\text{ext}}, \tag{68}$$

where

$$G^{\text{dyn}} = \int_\Omega (\delta\mathbf{r}\cdot\rho A\partial_t\mathbf{v} + \delta\varphi\rho I\partial_t\omega)\,\mathrm{d}s, \tag{69a}$$

$$G^{\text{int}} = \int_\Omega (\delta\boldsymbol{\Gamma}\cdot\mathbf{N} + \delta\kappa M)\,\mathrm{d}s, \tag{69b}$$

$$G^{\text{ext}} = \int_\Omega (\delta\mathbf{r}\cdot\overline{\mathbf{n}} + \delta\varphi\overline{m})\,\mathrm{d}s + [\delta\mathbf{r}\cdot\mathbf{n}_N + \delta\varphi\, m_N]_{\partial\Omega_N}. \tag{69c}$$

Accordingly, G^{dyn} contains the contribution of the inertia terms to the virtual work, G^{int} represents the virtual work due to deformations and G^{ext} accounts for the virtual work of external loads. The mid-point type temporal discretization in [39] can now be written as

$$G_{\text{mp}}^{\text{dyn}} + h G_{\text{mp}}^{\text{int}} = h G_{\text{mp}}^{\text{ext}}, \tag{70}$$

where

$$G_{\text{mp}}^{\text{dyn}} = \int_\Omega (\delta\mathbf{r}\cdot\rho A\,(\mathbf{v}_{n+1} - \mathbf{v}_n) + \delta\varphi\rho I\,(\omega_{n+1} - \omega_n))\,\mathrm{d}s, \tag{71a}$$

$$G_{\text{mp}}^{\text{int}} = \int_{\Omega} \left(\delta\mathbf{\Gamma}_{\text{alg}} \cdot \mathbf{N}_{n+1/2} + \partial_s(\delta\varphi) M_{n+1/2} \right) \mathrm{d}s, \tag{71b}$$

$$G_{\text{mp}}^{\text{ext}} = \int_{\Omega} \left(\delta\mathbf{r} \cdot \overline{\mathbf{n}}_{n+1/2} + \delta\varphi\, \overline{m}_{n+1/2} \right) \mathrm{d}s + \left[\delta\mathbf{r} \cdot (\mathbf{n}_{\text{N}})_{n+1/2} + \delta\varphi\, (m_{\text{N}})_{n+1/2} \right]_{\partial\Omega_{\text{N}}}. \tag{71c}$$

The two changes compared to the standard mid-point rule concern (i) the introduction of average stress-resultants in (71b), and (ii) the definition of $\delta\mathbf{\Gamma}_{\text{alg}}$ in (71b). Since in [39] St. Venant-Kirchhoff type material is considered (cf. Remark 2.1 in the present work), the average stress-resultants take the form

$$\mathbf{N}_{n+1/2} = \mathbf{D}_{\text{ts}}\mathbf{\Gamma}_{n+1/2} \quad \text{and} \quad M_{n+1/2} = EI\kappa_{n+1/2}, \tag{72}$$

where

$$\mathbf{\Gamma}_{n+1/2} = \frac{1}{2} \left(\mathbf{\Lambda}(\varphi_{n+1})^{\top} \partial_s \mathbf{r}_{n+1} + \mathbf{\Lambda}(\varphi_n)^{\top} \partial_s \mathbf{r}_n \right) - \mathbf{e}_1 \quad \text{and} \quad \kappa_{n+1/2} = \partial_s\varphi_{n+1/2}. \tag{73}$$

The definition of $\delta\mathbf{\Gamma}_{\text{alg}}$ can be motivated by the specific form of (66) along with (61a)–(61b), such that

$$\delta\mathbf{\Gamma}_{\text{alg}} := \delta\varphi Z_2(\Delta\varphi)\mathbf{\Lambda}(\varphi_{n+1/2})^{\top}\mathbf{S}\,\partial_s\mathbf{r}_{n+1/2} + Z_1(\Delta\varphi)\mathbf{\Lambda}(\varphi_{n+1/2})^{\top}\partial_s(\delta\mathbf{r}). \tag{74}$$

Inserting (74) into (71b), we obtain

$$G_{\text{mp}}^{\text{int}} = \int_{\Omega} \Big(\delta\varphi Z_2(\Delta\varphi)\partial_s\mathbf{r}_{n+1/2} \cdot \mathbf{S}^{\top}\mathbf{\Lambda}(\varphi_{n+1/2})\mathbf{N}_{n+1/2} \\ + \partial_s(\delta\mathbf{r}) \cdot Z_1(\Delta\varphi)\mathbf{\Lambda}(\varphi_{n+1/2})\mathbf{N}_{n+1/2} + \partial_s(\delta\varphi)M_{n+1/2} \Big) \mathrm{d}s. \tag{75}$$

It is now a straightforward exercise to show that (75) leads to the element internal force vector in equation (17) of [39] associated with a 2-node element based on linear Lagrangian shape functions.

To summarize, the displacement-based EM scheme devised in [39] is based on the fields $(\mathbf{r}, \varphi)$ and $(\mathbf{v}, \omega)$ and a mid-point type temporal discretization leading to (61a)–(61b) along with (70). The only modifications made in [39] to the standard mid-point rule are contained in (75), resulting in a specific EM scheme. Concerning the spatial discretization in [39], the well-established 2-node element is applied which relies on reduced one-point quadrature to alleviate transverse shear locking. Inspired by the investigations in this section, we next reduce our newly devised PH-EM scheme to displacement-based form in order to underline the main differences between our approach and that by Stander & Stein [39].

4.4.3 Irreducible PH-EM scheme

The present PH approach to the planar beam formulation leads in a natural way to a mixed formulation that facilitates the straightforward construction of a new EM scheme. In this section, we show that the mixed formulation can be reduced to a displacement-based formulation closely related to the one considered in Sect. 4.4.2. In analogy to (61a)–(61b), we consider the standard midpoint rule for $\partial_t\mathbf{r} = \mathbf{v}$ and $\partial_t\varphi = \omega$. Note that this essentially coincides with the weak counterparts (56a) and (56b). Furthermore, (56c) and (56d) can be recast in a form similar to (70) leading to

$$G_{\text{mp}}^{\text{dyn}} + h\tilde{G}_{\text{mp}}^{\text{int}} = hG_{\text{mp}}^{\text{ext}}, \tag{76}$$

where

$$\tilde{G}_{\mathrm{mp}}^{\mathrm{int}} = \int_{\Omega} \left(\delta\varphi \partial_s \mathbf{r}_{n+1/2} \cdot \mathbf{S}^\top \mathbf{\Lambda}(\varphi_{n+1/2}) \mathbf{N}_{n+1/2} + \partial_s(\delta\mathbf{r}) \cdot \mathbf{\Lambda}(\varphi_{n+1/2}) \mathbf{N}_{n+1/2} \right.$$
$$\left. + \partial_s(\delta\varphi) M_{n+1/2} \right) \mathrm{d}s. \tag{77}$$

Again, the formulas in (72) are used to calculate the algorithmic stress-resultants. However, instead of (73), the weak form (56a)–(56h) gives rise to

$$\mathbf{\Gamma}_{n+1/2} = \frac{1}{2} \left(\mathbf{\Gamma}_n + \mathbf{\Gamma}_{n+1} \right)$$
$$= \mathbf{\Gamma}_n + \frac{1}{2} \left(\Delta\varphi \mathbf{\Lambda}(\varphi_{n+1/2})^\top \mathbf{S} \partial_s \mathbf{r}_{n+1/2} + \mathbf{\Lambda}(\varphi_{n+1/2})^\top \partial_s(\Delta\mathbf{r}) \right), \tag{78a}$$

$$\kappa_{n+1/2} = \partial_s \varphi_{n+1/2}, \tag{78b}$$

see also (64). Comparison of (78a)–(78b) with (73) reveals that a crucial difference between the two EM schemes under consideration lies in the calculation of $\mathbf{\Gamma}_{n+1/2}$. Note that in the displacement-based formulation the calculation of $\mathbf{\Gamma}_{n+1/2}$ in (78a) requires to retrieve $\mathbf{\Gamma}_n$. Accordingly, $\mathbf{\Gamma}_n$ can be regarded as history variable for the calculation of the algorithmic stress-resultants. We further stress that the present EM scheme does not necessitate the introduction of the highly-nonlinear correction terms $Z_1(\Delta\varphi)$ and $Z_2(\Delta\varphi)$ featuring in (75).

5 Numerical results & discussion

In the following, the newly proposed approach is applied to some numerical examples. Since this involves the solution of the implicit set of equations (52) and (53), Newton's method is used in every time step. The spatial integrals are approximated by means of a full two-point Gaussian quadrature rule. The Dirichlet boundary conditions for the displacements and velocities are incorporated directly into the ansatz functions, see Remark 3.4. The computations have been performed using the finite element code moofeKIT, see [53], which can also be used for verification.

The first example is used to verify the discrete conservation properties. The second application demonstrates the ability to perform quasi-static simulations as well and shows that the PH approach mitigates numerical locking effects. The last example illustrates the usage of the proposed approach for interconnected flexible multibody systems.
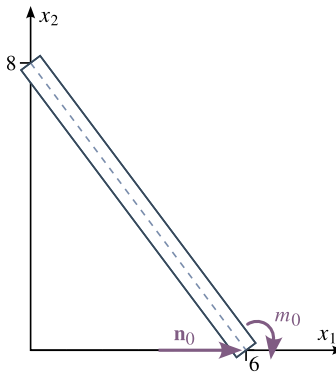
5.1 Flying spaghetti

The first example is concerned with the free motion of a tumbling beam. The so-called *flying spaghetti* problem was originally proposed by [54] and analyzed in multiple works, e.g. [55, 56]. The main objective here is to validate the time-discrete conservation principles of the proposed method. Initially positioned in an inclined configuration (see depiction in Table 1), the beam is released and allowed to move freely in space. The beam is subject to pure Neumann boundary conditions: A free end at $s = 0$ and a nodal force and torque at $s = L$, which is applied for a short period of time, i.e. $\mathbf{n}(s = L, t) = \mathbf{n}_0$ and $m(s = L, t) = m_0$ with

$$\mathbf{n}_0 = \begin{cases} 8\mathbf{e}_1 & \text{for } t \le 2.5, \\ 0 & \text{for } t > 2.5, \end{cases} \qquad m_0 = \begin{cases} -80 & \text{for } t \le 2.5, \\ 0 & \text{for } t > 2.5. \end{cases} \tag{79}$$

Table 1 Initial configuration, input loads and parameters for flying spaghetti problem

h	T	n_e	L	ρA	ρI	$EA = GA$	EI
0.1	15	10	10	1	10	10,000	100

At $t = 2.5$, the system is closed as both boundary inputs become zero and the beam continues with a free flight. Although the original parameters from [54] violate some physical plausibility relations (e.g. $EA/EI \neq \rho A/\rho I$), we use them here for the sake of comparability to many other works in the literature, see Table 1.

Firstly, we can verify that the motion is in good agreement with [54, Fig. 4], see snapshots in Fig. 4. Secondly, we can observe the conservation of energy and angular momentum in Figs. 5 and 6, respectively. The accuracy is of the order of machine precision. This verifies
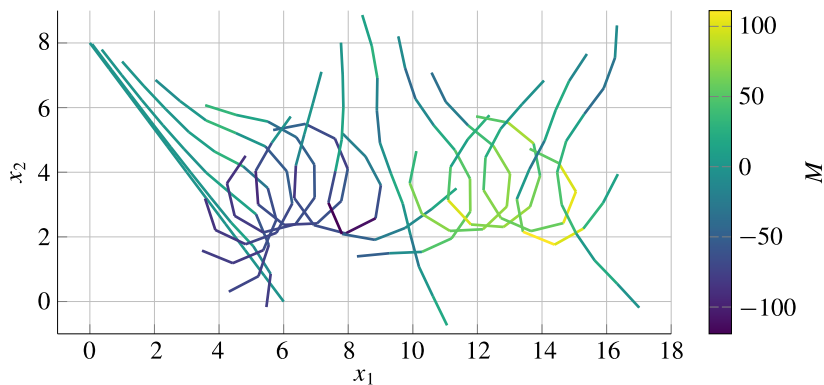
Fig. 4 Configuration of the beam at different time instances for $t \leq 7.5$, after each 5 time increments
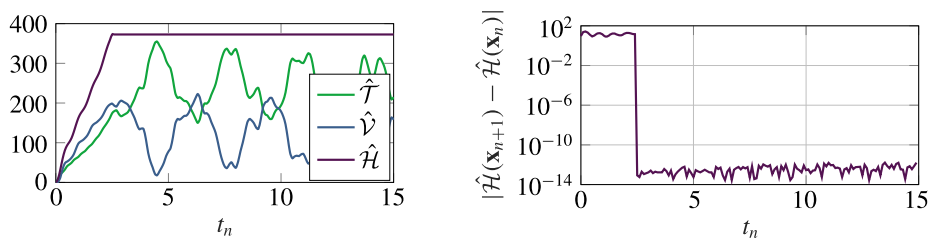
Fig. 5 Energetic evolution (left) and increments of total energy (right)
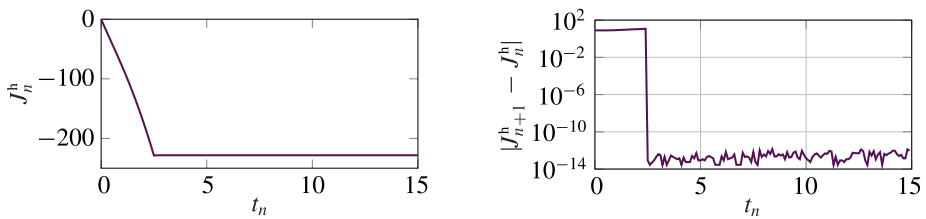
Fig. 6 Angular momentum evolution (left) and increments (right)

our previous findings that as soon as the system is closed both quantities are preserved. Note that also during the loading phase, consistent discrete-time balance equations have been obtained, see (55) and (60).

5.2 Quasi-static roll up

In this example, the ability of the proposed formulation to circumvent shear locking is demonstrated using a widespread benchmark problem, see e.g. [16, 57–59]. Moreover, it is shown that the proposed formulation is amenable to quasi-static simulations.

An initially straight cantilever beam, which is clamped at $s = 0$ such that we enforce the Dirichlet boundary conditions

$$\mathbf{r}(s=0,t)=\mathbf{0}, \quad \mathbf{v}(s=0,t)=\mathbf{0}, \quad \varphi(s=0,t)=0, \quad \omega(s=0,t)=0, \quad (80)$$

is rolled up by applying a quasi-static torque at the free end at $s = L$, see depiction in Table 2. A reference solution shows that for a torque of $m_{\text{rollup}} = 2\pi EI/L$, the beam is rolled up to a complete circular arc with constant curvature. For the simulation parameters we have chosen the same values as in [57], see Table 2.

Simulations for this benchmark problem yield incorrect outcomes when the numerical approximation procedure suffers from locking effects [57], since the stiffness is greatly over-estimated, resulting in the beam failing to form a complete ring. As this behavior is absent even with the coarse spatial discretization that we have chosen here, it can be concluded that shear locking does not occur in our PH beam model, see Fig. 7 (left). Contrarily, the final configuration obtained with the classical beam formulation by [39] - see also Sect. 4.4 - and a full two point Gaussian quadrature exhibits locking, see dashed line. This formulation requires a reduced integration with only one integration point to alleviate the problem.

Since our PH formulation is intrinsically dynamical, we refrain from introducing a static formulation and instead achieve a quasi-static simulation approach by neglecting inertial terms, such that $\rho = 0$. In this context, velocity-type quantities can then be regarded as *coordinate increments*. Moreover, time $t \in [0, 1]$ now corresponds to a loading factor which is increased in each step such that

$$m_0(t) = t \cdot m_{\text{rollup}}. \quad (81)$$

Table 2 Initial configuration, input torque and parameters for roll up example

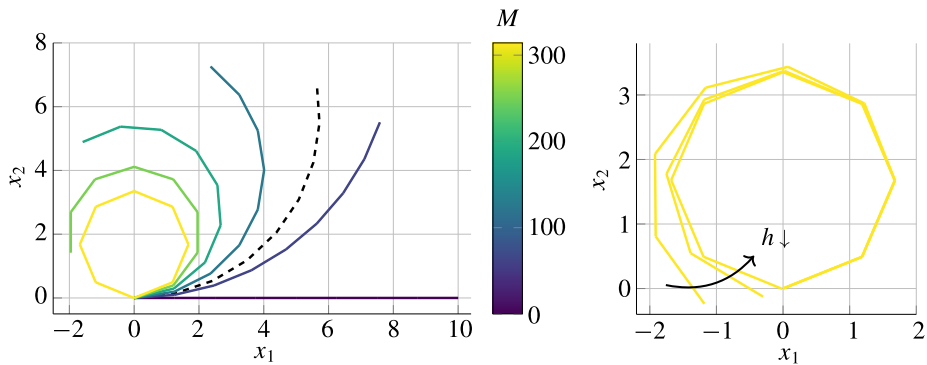| h	T	n_e	L	$\rho A = \rho I$	$EA = GA$	EI
0.01	1	8	10	0	10,000	500

Fig. 7 Configuration of the beam at different load levels $t \in \{0, 0.2, 0.2, 0.6, 0.8, 1\}$ obtained with our formulation and comparison with fully integrated classical formulation [39] (see dashed line) (left) and with different coarser discretization levels, $h \in \{0.02, 0.1, 0.2\}$ (right)

For $t = 1$, the final state is obtained, yielding a complete roll up of the cantilever beam. Due to the incrementing nature of our solution procedure, where approximation errors are induced in each *pseudo-time* step, a path-dependency becomes present. The approximate solution converges to the analytical solution when choosing sufficiently many pseudo-time steps, highlighting that the present approach is free from the numerical shear locking effect. See e.g. Fig. 7 for different configurations throughout the simulation. It can be verified that the beam has a homogeneous internal moment at each step. At the end of the simulation the end moment of $m_{\mathrm{rollup}} = 100\pi$ is exactly reached.

5.3 Closed loop flexible multibody system

Lastly, the well-known four-bar mechanism as a benchmark problem for flexible multibody systems, see e.g. [60–62], is analyzed. The compliant mechanism consists of three flexible beam elements with quadratic cross section and material parameters of steel, see Table 3 for details corresponding to [60]. The beams are interconnected by revolute joints, start from being at rest in an initial configuration as depicted in Table 3. The system is subject to gravity acting in negative x_2-direction, which is easily incorporated into the proposed PH formulation by setting the distributed input forces to the appropriate constant value, i.e. $\bar{\mathbf{n}} = \mathbf{g}$. Beam 1 and 3 are connected to the ground via revolute support joints.

We start our analysis by examining the evolution of the position of the center point P of the middle beam, initially located at $\mathbf{r}_P(t = 0) = (2.75, 1.5)$, over time. Here, we distinguish between two different scenarios: The first scenario deals with the chosen material parameters

Table 3 Initial configuration and parameters for multibody example

h	T	n_{e}	L	ρ
0.02	10	$\{10, 6, 6\}$	$\{\sqrt{5}, 1.5, \sqrt{2}\}$	2710

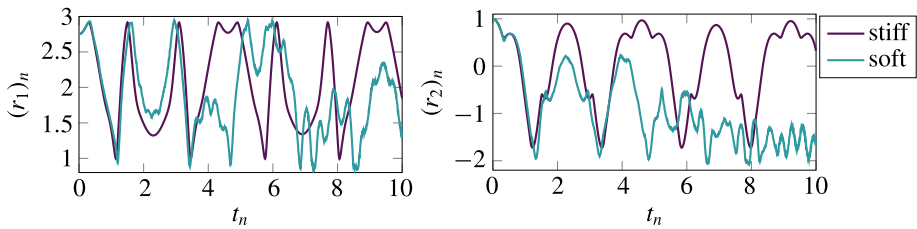| A	I	E	ν	$\mathbf{g}$
0.05^2	$0.05^4/12$	$2.1 \cdot 10^{11}$	0.3	$-9.81\rho A \mathbf{e}_2$
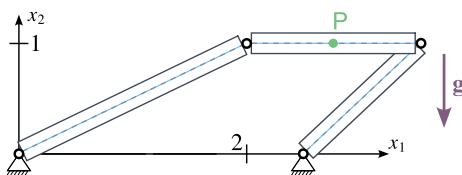
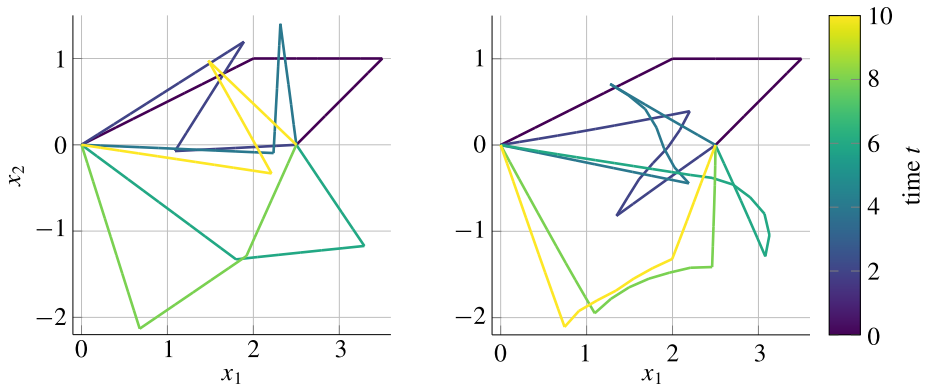**Fig. 8** Position of P over time

Fig. 9 Snapshots of the multibody system, $t \in \{0, 2, 4, 6, 8, 10\}$ (left: stiff scenario, right: soft scenario)

as for steel (see Table 3, labeled as "stiff"). For the second scenario we have reduced the elastic modulus of the middle beam to $E = 2.1 \cdot 10^8$ (labeled as "soft"), which also required a smaller time step size of $h_{\text{soft}} = 0.005$. The results depicted in Fig. 8 show that the flexible mechanism undergoes a periodic swing motion with a period of approximately 4.7 when choosing the stiff material for all beams. Snapshots for the motion are shown in Fig. 9.

Additionally, convergence studies were performed to investigate the approximation accuracy for the position of point P at $t = 1$ with respect to both temporal and spatial discretization in the stiff scenario. The results in Fig. 10 show that the relative error

$$e = \frac{||\mathbf{r}_{\mathsf{P}}(t=1) - \mathbf{r}_{\text{ref},\mathsf{P}}(t=1)||}{||\mathbf{r}_{\text{ref},\mathsf{P}}(t=1)||} \tag{82}$$

obtained with our approach decreases with order two with increasing temporal resolution, which is in line with the expected behavior for the midpoint-type discretization. For the reference overkill solution, we have chosen $h = 0.005$. The classical method [39] yields very similar results.

Next, the spatial discretization error is investigated by varying the number of elements n_{e} with reference length L^e, for all beams, see Fig. 10 (right). The results show that the error decreases with order two with increasing spatial resolution. For the reference overkill solution, we have chosen $n_{\text{e}} = 96$ for beam 2 and $n_{\text{e}} = 160$ for beams 1 and 3.

Lastly, we observed an increased robustness of our mixed EM approach in the PH framework (labelled "PH-EM") compared to the classical scheme [39] (labelled "cl-EM"), resulting in a notably reduced amount of Newton iterations per time step, see Fig. 11. The
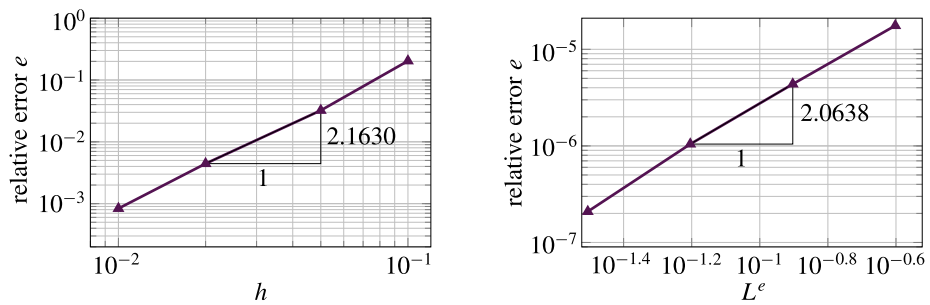
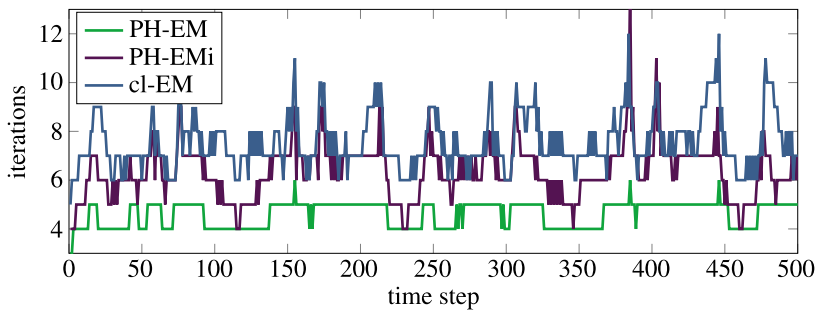**Fig. 10** Convergence results for accuracy of position of P

Fig. 11 Robustness comparison of necessary Newton iterations

mean number of necessary Newton iterations for the classical scheme is 6.464 compared to a number of 4.594 for our mixed approach PH-EM and 6.348 for its irreducible implementation (labelled "PH-EMi", see Sect. 4.4.3). This comparison has been performed with a less strict convergence criterion for the norm of the residual, i.e. $||\mathbf{Re}|| < 10^{-5}$. For smaller tolerances, cl-EM and PH-EMi do not converge anymore whereas PH-EM converged down to $||\mathbf{Re}|| < 10^{-11}$. For these investigations we have computed the tangent matrix for Newton's method using a central differences numerical approach.

6 Conclusion & outlook

In this work, we introduced a novel port-Hamiltonian (PH) formulation for planar geometrically exact beams, providing a structure-preserving approach to modeling their highly nonlinear dynamics. By leveraging mixed finite elements and second-order time-stepping methods, we ensured an exact discrete representation of energy and angular momentum balance, addressing a key challenge in the accurate and long-term simulation of flexible multibody systems. The continuous and discretized models are intrinsically passive, highlighting the potential of the PH framework for complex flexible multibody system simulations and advanced control design. We have also shown that the newly devised PH-EM scheme distinguishes itself from previously developed EM schemes. The distinguishing feature of the present PH-EM scheme has been highlighted by reducing the mixed PH-based formulation to an irreducible displacement-based version which shows that the implementation of the new EM scheme relies on the use of history variables. Furthermore, our numerical results

have demonstrated that the proposed formulation naturally mitigates shear locking, making it a robust and efficient choice for modeling large deformations and rotations in slender structures. Simulations validated the beneficial performance of the PH-based approach, with the energy-consistent discretization ensuring an exact energy balance in discrete time. The formulation accurately captures the nonlinear dynamics of planar geometrically exact beams while maintaining energy consistency and passivity, making it a promising tool for simulating and controlling flexible multibody systems.

Future research directions might explore the beneficial PH properties with respect to the energy-consistent interconnection in a multibody context. Moreover an extension of the PH modeling approach and the related design of an EM scheme to three-dimensional beam problems and other geometrically nonlinear mechanical systems can follow a similar procedure as in the present work. Lastly, also coupling with other fields, e.g. with electrical fields [63] or advanced dissipative terms [25, 64], may be included.

Appendix

A.1 Relation to a Hu-Washizu type variational formulation

The PH formulation dealt with in Sect. 3.1 can be linked to a mixed Hu-Washizu type extension of Hamilton's principle. To this end, we introduce the 8-field variational functional

$$
\begin{aligned}
S_{\mathrm{HW}}(\mathbf{r}, & \varphi, \mathbf{v}, \omega, \mathbf{\Gamma}, \kappa, \mathbf{N}, M) \\
&= \int_0^T \int_\Omega \left(\frac{1}{2} \rho A \mathbf{v} \cdot \mathbf{v} + \frac{1}{2} \rho I \omega^2 + (\partial_t \mathbf{r} - \mathbf{v}) \cdot \rho A \mathbf{v} + (\partial_t \varphi - \omega) \rho I \omega \right) \mathrm{d}s \, \mathrm{d}t \\
&\quad - \int_0^T \int_\Omega (W(\mathbf{\Gamma}, \kappa) + \mathbf{N} \cdot \mathbf{g}_1(\mathbf{\Gamma}, \varphi, \partial_s \mathbf{r}) + M g_2(\kappa, \partial_s \varphi)) \, \mathrm{d}s \, \mathrm{d}t \\
&\quad - \int_0^T V_{\mathrm{ext}}(\mathbf{r}, \varphi) \, \mathrm{d}t.
\end{aligned}
\tag{83}
$$

Therein, $\mathbf{N}$ and M act as Lagrange multipliers enforcing the kinematic constraints defining the strains in (5) and (6) such that

$$
\mathbf{g}_1(\mathbf{\Gamma}, \varphi, \partial_s \mathbf{r}) = \mathbf{\Lambda}(\varphi)^\top \partial_s \mathbf{r} - \mathbf{e}_1 - \mathbf{\Gamma} = \mathbf{0}, \qquad g_2(\kappa, \partial_s \varphi) = \partial_s \varphi - \kappa = 0,
\tag{84}
$$

and V_{ext} is the potential of external dead loads

$$
V_{\mathrm{ext}}(\mathbf{r}, \varphi) = - \int_\Omega (\overline{\mathbf{n}} \cdot \mathbf{r} + \overline{m} \varphi) \, \mathrm{d}s - [\mathbf{n}_{\mathrm{N}} \cdot \mathbf{r} + m_{\mathrm{N}} \varphi]_{\partial \Omega_N}.
\tag{85}
$$

It can be shown by a straightforward calculation that the stationary condition $\delta S_{\mathrm{HW}} = 0$ of functional (83) yields

$$
- (\delta \mathbf{r}, \rho A \partial_t \mathbf{v})_\Omega - (\partial_s (\delta \mathbf{r}), \mathbf{\Lambda N})_\Omega + [\delta \mathbf{r} \cdot \mathbf{n}_{\mathrm{N}}]_{\partial \Omega_{\mathrm{N}}} + (\delta \mathbf{r}, \overline{\mathbf{n}})_\Omega = 0,
\tag{86a}
$$

$$
- (\delta \varphi, \rho I \partial_t \omega)_\Omega - (\partial_s (\delta \varphi), M)_\Omega + \left(\delta \varphi, \partial_s \mathbf{r}^\top \mathbf{S} \mathbf{\Lambda N} \right)_\Omega + [\delta \varphi \, m_{\mathrm{N}}]_{\partial \Omega_{\mathrm{N}}} + (\delta \varphi, \overline{m})_\Omega = 0,
\tag{86b}
$$

$$
(\rho A \delta \mathbf{v}, \partial_t \mathbf{r} - \mathbf{v})_\Omega = 0,
\tag{86c}
$$

$$(\rho I \delta \omega, \partial_t \varphi - \omega)_\Omega = 0, \qquad (86\text{d})$$

$$(\delta \boldsymbol{\Gamma}, \mathbf{N} - \partial_{\boldsymbol{\Gamma}} W)_\Omega = 0, \qquad (86\text{e})$$

$$(\delta \kappa, M - \partial_\kappa W)_\Omega = 0, \qquad (86\text{f})$$

$$\left(\delta \mathbf{N}, \boldsymbol{\Gamma} - \boldsymbol{\Lambda}(\varphi)^\top \partial_s \mathbf{r} + \mathbf{e}_1\right)_\Omega = 0, \qquad (86\text{g})$$

$$(\delta M, \kappa - \partial_s \varphi)_\Omega = 0, \qquad (86\text{h})$$

for all $t \in [0, T]$. Apart from (86e) and (86f), which need to be replaced with weak forms of (17), these identities formally coincide with the weak form (34a)–(34h) of the PH formulation.

A.2 Implementation details for the basis functions and ansatz matrices

In Sect. 4.1 the displacements and velocities $(\mathbf{r}, \varphi, \mathbf{v}, \omega)$ are approximated in the following fashion:

$$\omega^h(s, t) = \sum_{i=1}^{n_\text{n}} N_i(s) \omega_i(t) \qquad (87)$$

$$= \begin{bmatrix} N_1(s) & N_2(s) & \cdots & N_{n_\text{n}}(s) \end{bmatrix} \begin{bmatrix} \omega_1(t) \\ \omega_2(t) \\ \vdots \\ \omega_{n_\text{n}}(t) \end{bmatrix} = \boldsymbol{\Phi}_1(s) \hat{\boldsymbol{\omega}}(t),$$

$$\mathbf{v}^h(s, t) = \sum_{i=1}^{n_\text{n}} N_i(s) \mathbf{v}_i(t) \qquad (88)$$

$$= \begin{bmatrix} N_1(s) & 0 & N_2(s) & 0 & \cdots & N_{n_\text{n}}(s) & 0 \\ 0 & N_1(s) & 0 & N_2(s) & \cdots & 0 & N_{n_\text{n}}(s) \end{bmatrix} \begin{bmatrix} \mathbf{v}_1(t) \\ \mathbf{v}_2(t) \\ \vdots \\ \mathbf{v}_{n_\text{n}}(t) \end{bmatrix}$$

$$= \boldsymbol{\Phi}_2(s) \hat{\mathbf{v}}(t),$$

cf. (41). The nodal basis functions $N_i(s)$ are defined as piecewise linear functions on the interval $[0, L]$, see Fig. 3. For the element-based degrees of freedom $(\boldsymbol{\Gamma}, \kappa)$ the ansatz is analogous but with piecewise constant basis functions $\tilde{N}_i(s)$, see Fig. 3. Since the computations are performed on element level in a reference element, these ansatz matrices have reference-element-related counterparts given by

$$\boldsymbol{\Phi}_1^{(e)}(\xi) = \begin{bmatrix} \hat{N}_1(\xi) & \hat{N}_2(\xi) \end{bmatrix},$$

$$\boldsymbol{\Phi}_2^{(e)}(\xi) = \begin{bmatrix} \hat{N}_1(\xi) & 0 & \hat{N}_2(\xi) & 0 \\ 0 & \hat{N}_1(\xi) & 0 & \hat{N}_2(\xi) \end{bmatrix} \qquad (89)$$

as well as

$$\boldsymbol{\Psi}_1^{(e)}(\xi) = 1 \quad \text{and} \quad \boldsymbol{\Psi}_2^{(e)}(\xi) = \begin{bmatrix} 1 & 0 \\ 0 & 1 \end{bmatrix}. \qquad (90)$$

A.3 System matrices for the finite-dimensional PH system

The approximation matrices arising in the spatial discretization procedure in Sect. 4.1 are given by

$$
\mathbf{M}_\alpha = \int_\Omega \mathbf{\Phi}_\alpha^\top \mathbf{\Phi}_\alpha \, \mathrm{d}s, \qquad \mathbf{C}_\alpha = \int_\Omega \mathbf{\Psi}_\alpha^\top \mathbf{\Psi}_\alpha \, \mathrm{d}s,
$$
$$
\mathbf{D}_2 = \int_\Omega \mathbf{\Psi}_2^\top \mathbf{D}_{\mathrm{ts}} \mathbf{\Psi}_2 \, \mathrm{d}s, \qquad \mathbf{D}_1 = \int_\Omega \mathbf{\Psi}_1^\top EI \mathbf{\Psi}_1 \, \mathrm{d}s
$$

(91)

for $\alpha \in \{1, 2\}$, as well as

$$
\mathbf{G}_1 = \int_\Omega \partial_s \mathbf{\Phi}_1^\top \mathbf{\Psi}_1 \, \mathrm{d}s, \qquad \mathbf{G}_2(\hat{\boldsymbol{\varphi}}) = \int_\Omega \partial_s \mathbf{\Phi}_2^\top \mathbf{\Lambda}(\varphi^{\mathrm{h}}) \mathbf{\Psi}_2 \, \mathrm{d}s,
$$
$$
\mathbf{V}(\hat{\mathbf{r}}, \hat{\boldsymbol{\varphi}}) = \int_\Omega \mathbf{\Phi}_1^\top (\partial_s \mathbf{r}^{\mathrm{h}})^\top \mathbf{S} \mathbf{\Lambda}(\varphi^{\mathrm{h}}) \mathbf{\Psi}_2 \, \mathrm{d}s.
$$

(92)

A.4 Implementation details for the boundary terms

In the finite-dimensional PH system (49), which arises after spatial discretization, the boundary terms require additional attention. The boundary terms are given by

$$
\mathbf{B}\hat{\mathbf{u}}(t) = \begin{bmatrix} \mathbf{B}_\partial & \mathbf{B}_\Omega \end{bmatrix} \begin{bmatrix} \mathbf{u}_\partial(t) \\ \hat{\mathbf{u}}_\Omega(t) \end{bmatrix},
$$

(93)

where for $\mathbf{u}_\partial$ we consider a boundary input vector for pure Neumann boundaries similar to the one in (31). The corresponding matrix is given by

$$
\mathbf{B}_\partial = \begin{bmatrix} \mathbf{0} & \mathbf{0} \\ \mathbf{0} & \mathbf{0} \\ \mathbf{B}_{\partial,n} & \mathbf{0} \\ \mathbf{0} & \mathbf{B}_{\partial,m} \\ \mathbf{0} & \mathbf{0} \\ \mathbf{0} & \mathbf{0} \end{bmatrix}, \quad \text{with } \mathbf{B}_{\partial,n} = \begin{bmatrix} \mathbf{I} & \mathbf{0} \\ \mathbf{0} & \mathbf{0} \\ \vdots & \vdots \\ \mathbf{0} & \mathbf{0} \\ \mathbf{0} & \mathbf{I} \end{bmatrix} \in \mathbb{R}^{2(n_{\mathrm{e}}+1)\times 4},
$$

$$
\mathbf{B}_{\partial,m} = \begin{bmatrix} 1 & 0 \\ 0 & 0 \\ \vdots & \vdots \\ 0 & 0 \\ 0 & 1 \end{bmatrix} \in \mathbb{R}^{(n_{\mathrm{e}}+1)\times 2}.
$$

(94)

Moreover in (93), the distributed input matrix and control input vector are given by

$$
\mathbf{B}_\Omega = \begin{bmatrix} \mathbf{0} & \mathbf{0} \\ \mathbf{0} & \mathbf{0} \\ \mathbf{M}_2 & \mathbf{0} \\ \mathbf{0} & \mathbf{M}_1 \\ \mathbf{0} & \mathbf{0} \\ \mathbf{0} & \mathbf{0} \end{bmatrix}, \quad \hat{\mathbf{u}}_\Omega(t) = \begin{bmatrix} \hat{\mathbf{u}}_{n,\Omega}(t) \\ \hat{\mathbf{u}}_{m,\Omega}(t) \end{bmatrix}
$$

(95)

containing the mass matrices $\mathbf{M}_1$ and $\mathbf{M}_2$ defined in (91). In the last equation, the discrete distributed input vector contains the nodal evaluations of the distributed control inputs (i.e. distributed forces and torques) such that

$$
\hat{\mathbf{u}}_{n,\Omega}(t) = \begin{bmatrix} \overline{\mathbf{n}}(s = 0, t) \\ \overline{\mathbf{n}}(s = \Delta s, t) \\ \vdots \\ \overline{\mathbf{n}}(s = n_{\mathrm{e}}\Delta s, t) \\ \overline{\mathbf{n}}(s = L, t) \end{bmatrix}, \quad \text{and} \quad \hat{\mathbf{u}}_{m,\Omega}(t) = \begin{bmatrix} \overline{m}(s = 0, t) \\ \overline{m}(s = \Delta s, t) \\ \vdots \\ \overline{m}(s = n_{\mathrm{e}}\Delta s, t) \\ \overline{m}(s = L, t) \end{bmatrix}, \quad (96)
$$

where Δs is the length of one finite element in the undeformed reference configuration such that $n_{\mathrm{e}}\Delta s = L$, the undeformed length of the beam. The collocated, and power-conjugated output corresponding to (93) can be deduced as

$$
\hat{\mathbf{y}} = \begin{bmatrix} \mathbf{y}_\partial \\ \hat{\mathbf{y}}_\Omega \end{bmatrix} = \begin{bmatrix} \mathbf{B}_\partial^\top \\ \mathbf{B}_\Omega^\top \end{bmatrix} \hat{\mathbf{z}}(\hat{\mathbf{x}}) = \begin{bmatrix} \mathbf{B}_{\partial,n}^\top \hat{\mathbf{v}} \\ \mathbf{B}_{\partial,m}^\top \hat{\boldsymbol{\omega}} \\ \mathbf{M}_2\hat{\mathbf{v}} \\ \mathbf{M}_1\hat{\boldsymbol{\omega}} \end{bmatrix} = \begin{bmatrix} \hat{\mathbf{v}}_1 \\ \hat{\mathbf{v}}_{n_{\mathrm{n}}} \\ \hat{\boldsymbol{\omega}}_1 \\ \hat{\boldsymbol{\omega}}_{n_{\mathrm{n}}} \\ \mathbf{M}_2\hat{\mathbf{v}} \\ \mathbf{M}_1\hat{\boldsymbol{\omega}} \end{bmatrix}, \quad (97)
$$

where the first 4 entries correspond to Neumann boundary inputs and the last 2 entries represent the distributed output depending on the nodal velocities.

A.5 Proof of the result in Sect. 4.4.2

Here, it is demonstrated that the modified midpoint discretization (66) yields a fulfillment of the kinematic relation (5) in the time endpoint t_{n+1}. Making use of (61a)–(61b), (66) can be written as

$$
\boldsymbol{\Gamma}_{n+1} - \boldsymbol{\Gamma}_n = \Delta\varphi Z_2(\Delta\varphi)\boldsymbol{\Lambda}(\varphi_{n+1/2})^\top \mathbf{S}\,\partial_s\mathbf{r}_{n+1/2} + Z_1(\Delta\varphi)\boldsymbol{\Lambda}(\varphi_{n+1/2})^\top \partial_s(\Delta\mathbf{r}), \quad (98)
$$

To prove that (98) does indeed yield the desired result, we make use of the identities

$$
\cos\frac{\Delta\varphi}{2}\boldsymbol{\Lambda}(\varphi_{n+1/2}) = \frac{1}{2}(\boldsymbol{\Lambda}_n + \boldsymbol{\Lambda}_{n+1}) =: \boldsymbol{\Lambda}_{n+1/2}, \quad (99a)
$$

$$
2\tan\frac{\Delta\varphi}{2}\mathbf{S}^\top \boldsymbol{\Lambda}_{n+1/2} = \boldsymbol{\Lambda}_{n+1} - \boldsymbol{\Lambda}_n, \quad (99b)
$$

where we write shortly $\boldsymbol{\Lambda}_n := \boldsymbol{\Lambda}(\varphi_n)$ and $\boldsymbol{\Lambda}_{n+1} := \boldsymbol{\Lambda}(\varphi_{n+1})$. The validity of (99a) and (99b) can be shown by using basic relations for the sine and cosine functions. Starting with the *sum-to-product* identities

$$
\cos x + \cos y = 2\cos\frac{x+y}{2}\cos\frac{x-y}{2}, \quad (100a)
$$

$$
\sin x - \sin y = 2\cos\frac{x+y}{2}\sin\frac{x-y}{2}, \quad (100b)
$$

together with $\cos a = \cos(-a)$ and $\sin a = -\sin(-a)$, the validity of (99a) can be checked on a component basis. For example, the $(1, 1)$ component of (99a) coincides with (100a) by

setting $x = \varphi_n$ and $y = \varphi_{n+1}$. The remaining component equations can be checked similarly. The second identity (99b) can be recast in the form

$$\sin \frac{\Delta\varphi}{2} \mathbf{S}^\top (\boldsymbol{\Lambda}_n + \boldsymbol{\Lambda}_{n+1}) = \cos \frac{\Delta\varphi}{2} (\boldsymbol{\Lambda}_{n+1} - \boldsymbol{\Lambda}_n) \tag{101}$$

Again, the validity of the last equation can be checked on a component basis. For example, the $(1, 2)$ component of (101) can be written as

$$-\sin \frac{y-x}{2} (\cos x + \cos y) = \cos \frac{y-x}{2} (-\sin y + \sin x), \tag{102}$$

where, as before, $x = \varphi_n$ and $y = \varphi_{n+1}$ has been set. Substituting (100a) and (100b) into the last equation confirms that (102) is identically satisfied. The remaining component equations of (99b) can be checked analogously. Now, (98) can be rewritten as

$$
\begin{aligned}
\boldsymbol{\Gamma}_{n+1} - \boldsymbol{\Gamma}_n &= \Delta\varphi \frac{\sin \frac{\Delta\varphi}{2}}{\frac{\Delta\varphi}{2}} \boldsymbol{\Lambda}(\varphi_{n+1/2})^\top \mathbf{S} \, \partial_s \mathbf{r}_{n+1/2} + \cos \frac{\Delta\varphi}{2} \boldsymbol{\Lambda}(\varphi_{n+1/2})^\top \partial_s (\Delta\mathbf{r}) \\
&= 2 \frac{\sin \frac{\Delta\varphi}{2}}{\cos \frac{\Delta\varphi}{2}} \boldsymbol{\Lambda}_{n+1/2}^\top \mathbf{S} \, \partial_s \mathbf{r}_{n+1/2} + \boldsymbol{\Lambda}_{n+1/2}^\top \partial_s (\Delta\mathbf{r}) \\
&= \left(\boldsymbol{\Lambda}_{n+1}^\top - \boldsymbol{\Lambda}_n^\top \right) \partial_s \mathbf{r}_{n+1/2} + \boldsymbol{\Lambda}_{n+1/2}^\top \partial_s (\Delta\mathbf{r}) \\
&= \boldsymbol{\Lambda}_{n+1}^\top \partial_s \mathbf{r}_{n+1} - \boldsymbol{\Lambda}_n^\top \partial_s \mathbf{r}_n.
\end{aligned}
$$

Here, in a first step (99a) has been used twice and in a second step (99b) has been applied. The last equation can be obtained by a direct calculation. Thus, provided that $\boldsymbol{\Gamma}_n = \boldsymbol{\Lambda}_n^\top \partial_s \mathbf{r}_n - \mathbf{e}_1$ is given, we obtain the desired result $\boldsymbol{\Gamma}_{n+1} = \boldsymbol{\Lambda}_{n+1}^\top \partial_s \mathbf{r}_{n+1} - \mathbf{e}_1$.

Author contributions PLK: Conceptualization, methodology, software, validation, formal analysis, investigation, data curation, writing–original draft preparation, writing–review and editing, visualization. PB: Conceptualization, methodology, validation, formal analysis, resources, writing–review and editing, supervision, project administration, funding acquisition. SRE: Validation, formal analysis, resources, writing–review and editing, supervision.

Code In order to enhance accessibility and reproducibility within the scientific community [65], the source code used for the computations has been made openly available at [53].

Declarations

Competing interests The authors declare no competing interests.

References

1. Shabana, A.A.: Flexible multibody dynamics: review of past and recent developments. Multibody Syst. Dyn. **1**(2), 189–222 (1997). https://doi.org/10.1023/A:1009773505418
2. Bauchau, O.A.: Flexible Multibody Dynamics. Solid Mechanics and Its Applications, vol. 176. Springer, Dordrecht (2011). https://doi.org/10.1007/978-94-007-0335-3
3. Simo, J.: A finite strain beam formulation. The three-dimensional dynamic problem. Part I. Comput. Methods Appl. Mech. Eng. **49**(1), 55–70 (1985). https://doi.org/10.1016/0045-7825(85)90050-7
4. Reissner, E.: On one-dimensional finite-strain beam theory: the plane problem. J. Appl. Math. Phys. **23**(5), 795–804 (1972). https://doi.org/10.1007/BF01602645
5. Antman, S.S.: Nonlinear Problems of Elasticity, 2nd edn. Applied Mathematical Sciences, vol. 107. Springer, New York (2005)
6. Cardona, A., Géradin, M.: A beam finite element non-linear theory with finite rotations. Int. J. Numer. Methods Eng. **26**(11), 2403–2438 (1988). https://doi.org/10.1002/nme.1620261105
7. Betsch, P., Steinmann, P.: Constrained dynamics of geometrically exact beams. Comput. Mech. **31**(1–2), 49–59 (2003). https://doi.org/10.1007/s00466-002-0392-1
8. Crisfield, M.A., Jelenić, G.: Objectivity of strain measures in the geometrically exact three-dimensional beam theory and its finite-element implementation. Proc. R. Soc. Lond., Ser. A, Math. Phys. Eng. Sci. **455**(1983), 1125–1147 (1999). https://doi.org/10.1098/rspa.1999.0352
9. Lang, H., Linn, J., Arnold, M.: Multi-body dynamics simulation of geometrically exact Cosserat rods. Multibody Syst. Dyn. **25**(3), 285–312 (2011). https://doi.org/10.1007/s11044-010-9223-x
10. Lang, H., Arnold, M.: Numerical aspects in the dynamic simulation of geometrically exact rods. Appl. Numer. Math. **62**(10), 1411–1427 (2012). https://doi.org/10.1016/j.apnum.2012.06.011
11. Eugster, S., Hesch, C., Betsch, P., Glocker, C.: Director-based beam finite elements relying on the geometrically exact beam theory formulated in skew coordinates. Int. J. Numer. Methods Eng. **97**(2), 111–129 (2014). https://doi.org/10.1002/nme.4586
12. Leyendecker, S., Betsch, P., Steinmann, P.: Objective energy–momentum conserving integration for the constrained dynamics of geometrically exact beams. Comput. Methods Appl. Mech. Eng. **195**(19–22), 2313–2333 (2006). https://doi.org/10.1016/j.cma.2005.05.002
13. Harsch, J., Sailer, S., Eugster, S.R.: A total Lagrangian, objective and intrinsically locking-free Petrov–Galerkin SE(3) Cosserat rod finite element formulation. Int. J. Numer. Methods Eng. **124**(13), 2965–2994 (2023). https://doi.org/10.1002/nme.7236
14. Leitz, T., de Almagro, R.T.S.M., Leyendecker, S.: Multisymplectic Galerkin Lie group variational integrators for geometrically exact beam dynamics based on unit dual quaternion interpolation—no shear locking. Comput. Methods Appl. Mech. Eng. **374**, 113475 (2021). https://doi.org/10.1016/j.cma.2020.113475
15. Herrmann, M., Kotyczka, P.: Relative-kinematic formulation of geometrically exact beam dynamics based on Lie group variational integrators. Comput. Methods Appl. Mech. Eng. **432**, 117367 (2024). https://doi.org/10.1016/j.cma.2024.117367
16. Wasmer, P., Betsch, P.: A projection-based quaternion discretization of the geometrically exact beam model. Int. J. Numer. Methods Eng. **125**(20), e7538 (2024). https://doi.org/10.1002/nme.7538
17. Meier, C., Popp, A., Wall, W.A.: Geometrically exact finite element formulations for slender beams: Kirchhoff-Love theory versus Simo–Reissner theory. Arch. Comput. Methods Eng. **26**(1), 163–243 (2019). https://doi.org/10.1007/s11831-017-9232-5
18. van der Schaft, A., Jeltsema, D.: Port-Hamiltonian systems theory: an introductory overview. Found. Trends Syst. Control **1**(2–3), 173–378 (2014). https://doi.org/10.1561/2600000002
19. Duindam, V., Macchelli, A., Stramigioli, S., Bruyninckx, H.: Modeling and Control of Complex Physical Systems: The Port-Hamiltonian Approach. Springer, Berlin (2009). https://doi.org/10.1007/978-3-642-03196-0
20. van Der Schaft, A., Maschke, B.: Hamiltonian formulation of distributed-parameter systems with boundary energy flow. J. Geom. Phys. **42**(1–2), 166–194 (2002). https://doi.org/10.1016/S0393-0440(01)00083-3
21. Jacob, B., Zwart, H.J.: Linear Port-Hamiltonian Systems on Infinite-Dimensional Spaces. Springer, Basel (2012)
22. Rashad, R., Califano, F., van der Schaft, A., Stramigioli, S.: Twenty years of distributed port-Hamiltonian systems: a literature review. IMA J. Math. Control Inf. **37**(4), 1400–1422 (2020). https://doi.org/10.1093/imamci/dnaa018
23. Thoma, T., Kotyczka, P.: Port-Hamiltonian FE models for filaments. IFAC-PapersOnLine **55**(30), 353–358 (2022). https://doi.org/10.1016/j.ifacol.2022.11.078
24. Kinon, P.L., Thoma, T., Betsch, P., Kotyczka, P.: Port-Hamiltonian formulation and structure-preserving discretization of hyperelastic strings. In: Proceedings of the 11th ECCOMAS Thematic Conference on Multibody Dynamics. Lisbon, Portugal, pp. 1–10 (2023). https://doi.org/10.48550/arXiv.2304.10957

25. Kinon, P.L., Thoma, T., Betsch, P., Kotyczka, P.: Generalized Maxwell viscoelasticity for geometrically exact strings: nonlinear port-Hamiltonian formulation and structure-preserving discretization. IFAC-PapersOnLine **58**(6), 101–106 (2024). https://doi.org/10.1016/j.ifacol.2024.08.264

26. Brugnoli, A., Alazard, D., Pommier-Budinger, V., Matignon, D.: Port-Hamiltonian formulation and symplectic discretization of plate models part I: Mindlin model for thick plates. Appl. Math. Model. **75**, 940–960 (2019). https://doi.org/10.1016/j.apm.2019.04.035

27. Brugnoli, A., Alazard, D., Pommier-Budinger, V., Matignon, D.: Port-Hamiltonian formulation and symplectic discretization of plate models part II: Kirchhoff model for thin plates. Appl. Math. Model. **75**, 961–981 (2019). https://doi.org/10.1016/j.apm.2019.04.036

28. Macchelli, A., Melchiorri, C.: Modeling and control of the Timoshenko beam. The distributed port Hamiltonian approach. SIAM J. Control Optim. **43**(2), 743–767 (2004). https://doi.org/10.1137/S0363012903429530

29. Golo, G., van der Schaft, A., Stramigioli, S.: Hamiltonian formulation of planar beams. IFAC Proc. Vol. **36**(2), 147–152 (2003). https://doi.org/10.1016/S1474-6670(17)38882-1

30. Macchelli, A., Melchiorri, C., Stramigioli, S.: Port-based modeling of a flexible link. IEEE Trans. Robot. **23**(4), 650–660 (2007). https://doi.org/10.1109/TRO.2007.898990

31. Ponce, C., Wu, Y., Le Gorrec, Y., Ramirez, H.: Port-Hamiltonian modeling of a geometrically nonlinear hyperelastic beam. IFAC-PapersOnLine **58**(6), 309–314 (2024). https://doi.org/10.1016/j.ifacol.2024.08.299

32. Thoma, T., Kotyczka, P., Egger, H.: On the velocity-stress formulation for geometrically nonlinear elastodynamics and its structure-preserving discretization. Math. Comput. Model. Dyn. Syst. **30**(1), 701–720 (2024). https://doi.org/10.1080/13873954.2024.2397486

33. Brugnoli, A., Matignon, D., Morlier, J.: A linearly-implicit energy preserving scheme for geometrically nonlinear mechanics based on non-canonical Hamiltonian formulations (2025). arXiv [math.NA] arXiv:2503.04695

34. Brugnoli, A., Alazard, D., Pommier-Budinger, V., Matignon, D.: Port-Hamiltonian flexible multibody dynamics. Multibody Syst. Dyn. **51**(3), 343–375 (2021). https://doi.org/10.1007/s11044-020-09758-6

35. Caasenbrood, B., Pogromsky, A., Nijmeijer, H.: Energy-shaping controllers for soft robot manipulators through port-Hamiltonian Cosserat models. SN Comput. Sci. **3**(6), 494 (2022). https://doi.org/10.1007/s42979-022-01373-w

36. Cardoso-Ribeiro, F.L., Matignon, D., Lefèvre, L.: A partitioned finite element method for power-preserving discretization of open systems of conservation laws. IMA J. Math. Control Inf. **38**(2), 493–533 (2021). https://doi.org/10.1093/imamci/dnaa038

37. Warsewa, A., Böhm, M., Sawodny, O., Tarín, C.: A port-Hamiltonian approach to modeling the structural dynamics of complex systems. Appl. Math. Model. **89**, 1528–1546 (2021). https://doi.org/10.1016/j.apm.2020.07.038

38. Brugnoli, A., Rashad, R., Califano, F., Stramigioli, S., Matignon, D.: Mixed finite elements for port-Hamiltonian models of von Kármán beams. IFAC-PapersOnLine **54**(19), 186–191 (2021). https://doi.org/10.1016/j.ifacol.2021.11.076

39. Stander, N., Stein, E.: An energy-conserving planar finite beam element for dynamics of flexible mechanisms. Eng. Comput. **13**(6), 60–85 (1996). https://doi.org/10.1108/02644409610128418

40. Ibrahimbegović, A., Mamouri, S.: Nonlinear dynamics of flexible beams in planar motion: formulation and time-stepping scheme for stiff problems. Comput. Struct. **70**(1), 1–22 (1999). https://doi.org/10.1016/S0045-7949(98)00150-3

41. Brugnoli, A.: A Port-Hamiltonian Formulation of Flexible Structures. Modelling and Structure-Preserving Finite Element Discretization. PhD thesis, France, Université de Toulouse, ISAE-SUPAERO (2020)

42. Mehrmann, V., Morandin, R.: Structure-preserving discretization for port-Hamiltonian descriptor systems. In: 2019 IEEE 58th Conference on Decision and Control (CDC), pp. 6863–6868. IEEE (2019). https://doi.org/10.1109/CDC40024.2019.9030180

43. Beattie, C., Mehrmann, V., Xu, H., Zwart, H.: Linear port-Hamiltonian descriptor systems. Math. Control Signals Syst. **30**, 1–27 (2018). https://doi.org/10.1007/s00498-018-0223-3

44. Mehrmann, V., Unger, B.: Control of port-Hamiltonian differential-algebraic systems and applications. Acta Numer. **32**, 395–515 (2023). https://doi.org/10.1017/S0962492922000083

45. Kinon, P.L., Thoma, T., Betsch, P., Kotyczka, P.: Discrete nonlinear elastodynamics in a port-Hamiltonian framework. PAMM **23**(3), e202300144 (2023). https://doi.org/10.1002/pamm.202300144

46. Brugnoli, A., Cardoso-Ribeiro, F.L., Haine, G., Kotyczka, P.: Partitioned finite element method for structured discretization with mixed boundary conditions. IFAC-PapersOnLine **53**(2), 7557–7562 (2020). https://doi.org/10.1016/j.ifacol.2020.12.1351

47. Thoma, T., Kotyczka, P.: Explicit port-Hamiltonian FEM-models for linear mechanical systems with non-uniform boundary conditions. IFAC-PapersOnLine **55**(20), 499–504 (2022). https://doi.org/10.1016/j.ifacol.2022.09.144

48. Brugnoli, A., Haine, G., Matignon, D.: Explicit structure-preserving discretization of port-Hamiltonian systems with mixed boundary control. IFAC-PapersOnLine **55**(30), 418–423 (2022). https://doi.org/10.1016/j.ifacol.2022.11.089

49. Zienkiewicz, O.C., Taylor, R.L., Zhu, J.Z.: The Finite Element Method: Its Basis and Fundamentals, 6th edn. Elsevier, Heidelberg (2010). Reprint., transferred to digital print

50. Wriggers, P.: Nonlinear Finite Element Methods. Springer, Berlin (2008). https://doi.org/10.1007/978-3-540-71001-1

51. Hairer, E., Lubich, C., Wanner, G.: Geometric Numerical Integration. Springer, Berlin (2006). https://doi.org/10.1007/3-540-30666-8

52. Gonzalez, O.: Time integration and discrete Hamiltonian systems. J. Nonlinear Sci. **6**(5), 449–467 (1996). https://doi.org/10.1007/BF02440162

53. Franke, M., Zähringer, F., Hille, M., Kinon, P.L., Reiff, P.: MoofeKIT: MATLAB object-oriented finite element KIT, v1.0.3. Version v1.0.3 (2025). https://doi.org/10.5281/zenodo.15044922

54. Simo, J.C., Vu-Quoc, L.: On the dynamics of flexible beams under large overall motions—the plane case: part II. J. Appl. Mech. **53**(4), 855–863 (1986). https://doi.org/10.1115/1.3171871

55. Hsiao, K.-M., Jang, J.-Y.: Dynamic analysis of planar flexible mechanisms by co-rotational formulation. Comput. Methods Appl. Mech. Eng. **87**(1), 1–14 (1991). https://doi.org/10.1016/0045-7825(91)90143-T

56. Gams, M., Planinc, I., Saje, M.: Energy conserving time integration scheme for geometrically exact beam. Comput. Methods Appl. Mech. Eng. **196**(17–20), 2117–2129 (2007). https://doi.org/10.1016/j.cma.2006.10.012

57. Hante, S., Tumiotto, D., Arnold, M.: A Lie group variational integration approach to the full discretization of a constrained geometrically exact Cosserat beam model. Multibody Syst. Dyn. **54**(1), 97–123 (2022). https://doi.org/10.1007/s11044-021-09807-8

58. Ren, H., Fan, W., Zhu, W.D.: An accurate and robust geometrically exact curved beam formulation for multibody dynamic analysis. J. Vib. Acoust. **140**(1), 011012 (2018). https://doi.org/10.1115/1.4037513

59. Campanelli, M., Berzeri, M., Shabana, A.A.: Performance of the incremental and non-incremental finite element formulations in flexible multibody problems. J. Mech. Des. **122**(4), 498–507 (2000). https://doi.org/10.1115/1.1289636

60. Yu, X., Zwölfer, A., Mikkola, A.: An efficient, floating-frame-of-reference-based recursive formulation to model planar flexible multibody applications. J. Sound Vib. **547**, 117542 (2023). https://doi.org/10.1016/j.jsv.2022.117542

61. Fan, W.: An efficient recursive rotational-coordinate-based formulation of a planar Euler–Bernoulli beam. Multibody Syst. Dyn. **52**(2), 211–227 (2021). https://doi.org/10.1007/s11044-021-09783-z

62. Berzeri, M., Campanelli, M., Shabana, A.A.: Definition of the elastic forces in the finite-element absolute nodal coordinate formulation and the floating frame of reference formulation. Multibody Syst. Dyn. **5**(1), 21–54 (2001). https://doi.org/10.1023/A:1026465001946

63. Huang, D., Leyendecker, S.: An electromechanically coupled beam model for dielectric elastomer actuators. Comput. Mech. **69**(3), 805–824 (2022). https://doi.org/10.1007/s00466-021-02115-0

64. Ferri, G., Ignesti, D., Marino, E.: An efficient displacement-based isogeometric formulation for geometrically exact viscoelastic beams. Comput. Methods Appl. Mech. Eng. **417**, 116413 (2023). https://doi.org/10.1016/j.cma.2023.116413

65. Ebel, H., et al.: Data publishing in mechanics and dynamics: challenges, guidelines, and examples from engineering design. Data-Cent. Eng. **6**, e23 (2025). https://doi.org/10.1017/dce.2025.13

Publisher's note Springer Nature remains neutral with regard to jurisdictional claims in published maps and institutional affiliations.